UNIVERSIDAD DE INVESTIGACIÓN DE TECNOLOGÍA EXPERIMENTAL YACHAY

Escuela de Ciencias Químicas e Ingeniería

TÍTULO: UV-ABSORPTION OF LIGNIN STRUCTURES EXTRACTED FROM AGRICULTURAL WASTES

Trabajo de integración curricular presentado como requisito para la obtención del título de Químico(a)

Autor:

María Belén Arcentales Vera

Tutor: Floralba López González, PhD.
Co-tutor: Alicia Sommer, PhD.

Urcuqui-Ecuador, Abril 2020

SECRETARÍA GENERAL
(Vicerrectorado Académico/Cancillería)
ESCUELA DE CIENCIAS QUÍMICAS E INGENIERÍA
CARRERA DE QUÍMICA
ACTA DE DEFENSA No. UITEY-CHE-2020-00017-AD

A los 3 días del mes de abril de 2020, a las 10:00 horas, de manera virtual mediante videoconferencia, y ante el Tribunal Calificador, integrado por los docentes:

Presidente Tribunal de Defensa	Dr. SAUCEDO VAZQUEZ, JUAN PABLO , Ph.D.
Miembro No Tutor	Dr. BASTARDO GONZÁLEZ, ERNESTO LUIS , Ph.D.
Tutor	Dra. LOPEZ GONZALEZ, FLORALBA AGGENY , Ph.D.

El(la) señor(ita) estudiante **ARCENTALES VERA, MARIA BELEN**, con cédula de identidad No. **1314852888**, de la **ESCUELA DE CIENCIAS QUÍMICAS E INGENIERÍA**, de la Carrera de **QUÍMICA**, aprobada por el Consejo de Educación Superior (CES), mediante Resolución **RPC-SO-39-No.456-2014**, realiza a través de videoconferencia, la sustentación de su trabajo de titulación denominado: **UV-Absorption of lignin structures extracted from agricultural wastes**, previa a la obtención del título de **QUÍMICO/A**.

El citado trabajo de titulación, fue debidamente aprobado por el(los) docente(s):

Tutor	Dra. LOPEZ GONZALEZ, FLORALBA AGGENY , Ph.D.
Co - Tutor	Dra. SOMMER MARQUEZ, ALICIA ESTELA , Ph.D.

Y recibió las observaciones de los otros miembros del Tribunal Calificador, las mismas que han sido incorporadas por el(la) estudiante.

Previamente cumplidos los requisitos legales y reglamentarios, el trabajo de titulación fue sustentado por el(la) estudiante y examinado por los miembros del Tribunal Calificador. Escuchada la sustentación del trabajo de titulación a través de videoconferencia, que integró la exposición de el(la) estudiante sobre el contenido de la misma y las preguntas formuladas por los miembros del Tribunal, se califica la sustentación del trabajo de titulación con las siguientes calificaciones:

Tipo	Docente	Calificación
Miembro Tribunal De Defensa	Dr. BASTARDO GONZÁLEZ, ERNESTO LUIS , Ph.D.	10,0
Tutor	Dra. LOPEZ GONZALEZ, FLORALBA AGGENY , Ph.D.	10,0
Presidente Tribunal De Defensa	Dr. SAUCEDO VAZQUEZ, JUAN PABLO , Ph.D.	9,5

Lo que da un promedio de: **9.8 (Nueve punto Ocho)**, sobre 10 (diez), equivalente a: **APROBADO**

Para constancia de lo actuado, firman los miembros del Tribunal Calificador, el/la estudiante y el/la secretario ad-hoc.

Certifico que *en cumplimiento del Decreto Ejecutivo 1017 de 16 de marzo de 2020, la defensa de trabajo de titulación (o examen de grado modalidad teórico práctica) se realizó vía virtual, por lo que las firmas de los miembros del Tribunal de Defensa de Grado, constan en forma digital.*

ARCENTALES VERA, MARIA BELEN
Estudiante

Dr. SAUCEDO VAZQUEZ, JUAN PABLO , Ph.D.
Presidente Tribunal de Defensa

Dra. LOPEZ GONZALEZ, FLORALBA AGGENY , Ph.D.
Tutor

Dr. BASTARDO GONZÁLEZ, ERNESTO LUIS , Ph.D.
Miembro No Tutor

ESCOBAR LANDAZURI, ANA MARIA
Secretario Ad-hoc

AUTORÍA

Yo, **María Belén Arcentales Vera**, con cédula de identidad 1314852888, declaro que las ideas, juicios, valoraciones, interpretaciones, consultas bibliográficas, definiciones y conceptualizaciones expuestas en el presente trabajo; asi cómo, los procedimientos y herramientas utilizadas en la investigación, son de absoluta responsabilidad de la autora de trabajo de integración curricular. Así mismo, me acojo a los reglamentos internos de la Universidad de Investigación de Tecnologia Experimental Yachay.

Urcuquí, julio 2020.
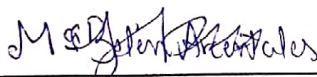

María Belén Arcentales Vera

CI: 1314852888

AUTORIZACIÓN DE PUBLICACIÓN

Yo, **María Belén Arcentales Vera**, con cédula de identidad 1314852888, cedo a la Universidad de Tecnología Experimental Yachay, los derechos de publicación de la presente obra, sin que deba haber un reconocimiento económico por este concepto. Declaro además que el texto del presente trabajo de titulación no podrá ser cedido a ninguna empresa editorial para su publicación u otros fines, sin contar previamente con la autorización escrita de la Universidad.

Asimismo, autorizo a la Universidad que realice la digitalización y publicación de este trabajo de integración curricular en el repositorio virtual, de conformidad a lo dispuesto en el Art. 144 de la Ley Orgánica de Educación Superior.

Urcuquí, julio 2020.

María Belén Arcentales Vera
CI: 1314852888

To my family,

for their unconditional love and support.

Acknowledgments

This thesis would not have been possible without the help of many people. First of all, I want to thank my parents for their support at every step of my life. Thank you mom for all your daily love and attention, despite the miles that separated us. To my sisters, Valeria and Melissa, for being my motivation and encouraging me to continue in difficult times. Thank you for such support, laughs and unforgettable moments. I also want to express my gratitude to my aunts, Gaby and Jimena, for their encouraging words and be my side in difficult times. To my sweet little niece Emily, for your fun games and sleepover nights.

I want to thank all the Yachay Tech teachers for the knowledge imparted and their guidance during my professional training. I gratefully thank my advisor, Floralba Lopez, for inspiring me and being a great mentor for the realization of this thesis. I also thank Alicia Sommer, for providing her help to characterize my thesis samples. My deepest gratitude to the investigator staff of the Institute of Materials Science of Madrid for their contribution and help during the data collection, especially to Miguel Camblor and Raquel Martin-Sampedro.

I want to thank the great friendships I made at this university. Thanks to all of you for those nights of studies, laughs, movies, meals, and parties we shared and for being now my Yachay Tech family. I especially thank Magno for his constant motivation and help during this last year.

María Belén Arcentales Vera

Resumen

La lignina es uno de los materiales naturales más abundantes en la naturaleza, la cual posee una estructura tridimensional muy compleja y ramificada. Contiene grupos funcionales que absorben rayos UV, convirtiendo a la lignina en un protector solar natural. Esta propiedad podría aprovecharse para minimizar el perjuicio de la exposición solar, que aumenta el daño biológico y la degradación de los compuestos orgánicos. En el presente trabajo, la lignina fue extraída de tallos de rosas y maíz, productos considerados como residuos agrícolas en Ecuador. La extracción se realizó mediante un tratamiento organosolv, y la caracterización fue estudiada a través de varias técnicas espectroscópicas, microscópicas y técnicas de difracción como FTIR, FE-SEM y EDX, DLS, Potencial Zeta- UV-VIS y XRD. Finalmente, fueron preparadas películas de alcohol polivinílico conteniendo pequeñas cantidades de lignina. Las películas fueron analizadas y los resultados mostraron una gran capacidad para absorber radiación UV. Las películas que contienen 2% y 4% de lignina, mostraron porcentajes de absorbancia de 98,05% y 99,75%, respectivamente. Además, la lignina fue agregada a cremas comerciales mostrando un incremento notables de absorbancia de 48% a 85,46%. Estos ensayos confirmaron que la lignina es una alternativa prometedora para el desarrollo de materiales debido a la excelente propiedad de absorción UV.

Palabras clave: *lignina, exposición solar, protección UV, películas de PVA, residuos agrícolas*

Abstract

Lignin is one of the most commonly available natural material which has a very complex and branched three-dimensional structure. It contains UV-absorbing functional groups that make it a natural sunscreen, which could be exploited to avoid the harmful sun exposure, that increases biological damage and degradation of organic compounds. In the present work, lignin was extracted from rose stems and corn stalks, two products considered agricultural waste material in Ecuador. The extraction was carried out using an organosolv treatment, and characterization was performed by several spectroscopic, microscopic, and diffraction techniques such as FTIR, FE-SEM and EDX, DLS, Zeta Potential, UV-VIS, and XRD. Finally, polyvinyl films containing low amounts of lignin were prepared. These prepared films were analyzed showing a high UV absorption ability. PVA-films containing 2% and 4% showed 98.05% and 99.75% of absorbance, respectively. Besides, lignin was added to a commercial cream showing an enhancement of UV absorbance from 48% to 85.46%. These assays showed that lignin is a promising alternative for the development of enhanced materials due to the great UV absorption property.

Keywords: *lignin, sun exposure, UV protection, PVA-films, agricultural wastes*

CONTENTS

LIST OF FIGURES

LIST OF TABLES

LIST OF ABBREVIATIONS

CL-1 Sample of corn lignin from filtrate phase

$\mathbf{D}_m$ Mean diameter of particles

DLS Dynamic light scattering

EDX Energy-dispersive X-ray spectroscopy

FTIR Fourier-transform infrared spectroscopy

G Guaiacyl unit

H p-hydroxy phenol unit

ICL1 Sample of insoluble corn lignin

IRL1 Sample of insoluble rose lignin

PDI Polydispersity index

pH Potential of Hydrogen

PVA Polyvinyl Alcohol

RL-1 Sample of rose lignin from filtrate phase

SEM Scanning electron microscope

SPF Sun protection factor

S Syringyl unit

UVA Ultraviolet A (long-wavelength between 320 and 400 nm)

UVB Ultraviolet B (shorter-wavelength range from 290 to 320 nm)

UVC Ultraviolet C (shorter wavelength between 100 and 290 nm)

UV Ultraviolet radiation

XRD X-ray diffraction

INTRODUCTION

Recently, extensive research has been done on lignocellulosic biomass as starting materials for the production of bio-materials because it is highly available from agricultural wastes, forest products, energy crops and so on. Agricultural biomass consists mainly of natural polymers such as cellulose, hemicellulose, and lignin. Cellulose has been used for a wide variety of potential applications. During its extraction, hemicellulose and lignin are usually discarded. However, hemicellulose and lignin also possess a huge potential for the production of green materials.[1] Lignin stands out as the only lignocellulosic compound with a structure rich in aromatic rings which contains UV-absorbing functional groups, such as phenolic units, ketones, and other chromophores[2] that make lignin an interesting material with excellent antioxidant and UV absorption properties.

As one of the leading countries for its agricultural production in Latin America, Ecuador generates a considerable amount of lignocellulosic agricultural wastes. Also, Ecuador occupies the top three of the world's largest producers and exporters of flowers, as well as, it has a high production of corn throughout all the country. Therefore, there is an imperative need to provide an added-value to wastes generated from these crops and produce competitive products.

This study seeks to take advantage of the antioxidant and UV absorption properties from lignin. It includes the extraction and characterization of lignin obtained from two different bio-sources of Province of Imbabura in Ecuador, through an organosolv treatment by using acetic and formic acid, and the preparation and characterization of polyvinyl alcohol (synthetic polymer) films containing low amounts of lignin. The experimental procedure of this research was conducted in Yachay Tech University laboratories while the characterization analyses were performed in the Instituto de Ciencia de Materiales de Madrid (ICMM).

In this research, the Chapter 1 provides background information in which some basic concepts are explained. This is followed by the problem statement and objectives in the Chapter 2 and 3, respectively. Then, in Chapter 4, it is explained the methodology employed and the different processes for the obtention of lignin and PVA- lignin films as well as the principles of the characterization methods used are described. In Chapter 5 are presented the obtained results of the extraction process, characterization of prepared material and tests carried out. Finally, the conclusions and suggestions for further experiments are presented.

CHAPTER 1

THEORETICAL FRAME

1.1 Lignocellulosic Biomass

Lignocellulosic biomass refers to residues obtained from forest products, agricultural waste, and energy crops. It is considered as the most available, economical and renewable natural resource in the world.[3] Lignocellulosic biomass is composed mainly of cellulose, hemicellulose, and lignin, which are natural polymers, also called bio-polymers. In addition, small percentages of organic extractives, and minerals can be found. Lignocellulose structure varies according to the bio-source[4], i.e. the amount of each lignocellulosic component depends on the type of biomass source.

Cellulose is the most abundant organic polymer on nature which exhibits a linear structure comprised of glucose monosaccharide units. Its chemical structure is represented for $(C_6H_{10}O_5)_n$. Cellulose molecules are linked in chains giving rise to the formation of microfibers and consequently the cellulose fibers. As a result of its large supramolecular structures, cellulose is insoluble in water and most common solvents. Its poor solubility is explained by the interactions between and within the cellulose polymer chains which are determined by hydrogen bonds.[5] *Hemicellulose* is a branched

heterogeneous polymer constituted by lateral chains of one or several sugar units. Unlike cellulose, hemicellulose has a low molecular weight. Also, hemicellulose is a much more soluble molecule than cellulose since, in addition to glucose, it is composed of water-soluble sugars.[6] The amount and type of monomers present in the hemicellulose structure depend on feedstock sources. Agricultural biomass is mainly composed of xylan sugars while wood hemicellulose is based on glucomannan units.[7] *Lignin* is the second bio-polymer with greater availability. It is found in the secondary cell wall of plants. Lignin is an amorphous material with a complex aromatic structure based on phenylpropanoid units.[8] It is a poorly soluble polymer in most solvents, as cellulose. Also, it is considered as a resin that holds lignocellulosic components together. Besides, there is a small percentage of inorganic minerals and organic extractives that include fats, waxes, alkaloids, proteins, phenolics, simple sugars, pectins, glycosides, saponins, and essential oils.[9] As shown in Figure 1.1, that cellulose fibers are surrounded by hemicellulose and lignin. Lignin provides a protective covering around cellulose and hemicellulose. Also, hemicellulose allows to join cellulose with lignin.[10]
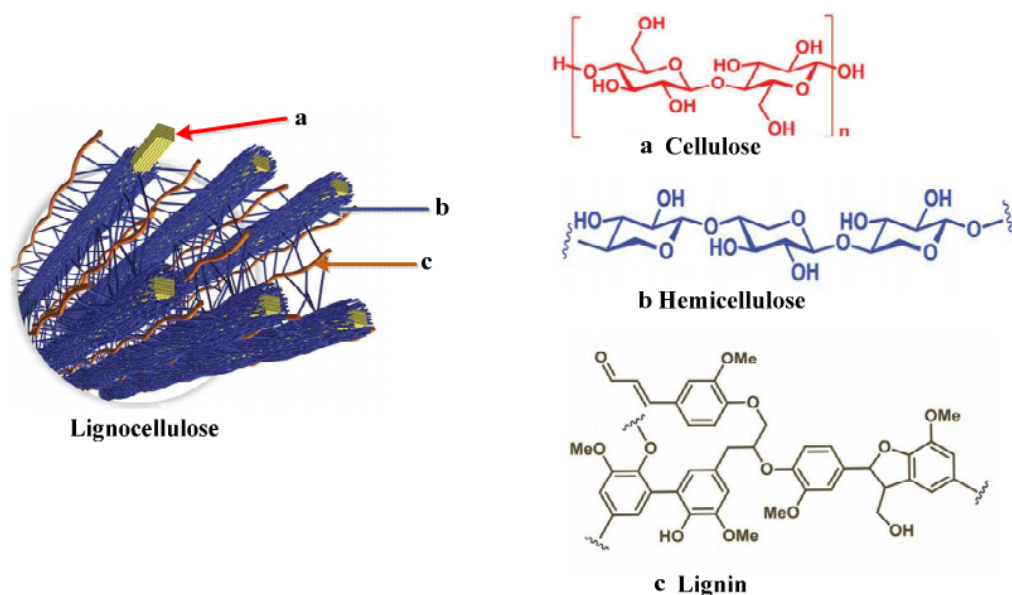
Figure 1.1: General representation of structure of lignocellulosic biomass.[11]

Literature reports that the composition of agricultural waste such as corn stover, consists of 33–35% wt. cellulose, 21–24% wt. hemicellulose and 17–22% wt. lignin.[12]

1.1.1 Lignin: Structure and biological functions in plants

Lignin has a very complex and branched three-dimensional structure build-up by three phenyl propane monomers called monolignols which are p-coumaryl, coniferyl and sinapyl alcohol which vary by their methylation degree. These units are bonded to each other through different linkages like ether and carbon-carbon bonds.[13] The polymerization of these monomers results in the formation of the building blocks in lignin: p-hydroxy phenol (H), guaiacyl (G), and syringyl (S) residues, respectively. These structures are represented in Figure 1.2. The proportion of each monolignol into the whole structure depends on the species of plant. For instance, guaiacyl (G) units are abundant in gymnosperms, hardwood consists mainly of guaiacyl (G) and syringyl (S), and the grasses are composed of the three monolignols (G, H, S).[14] The lignin structures reported in the different investigations are approximate models developed from the data obtained from the chemical analyses.
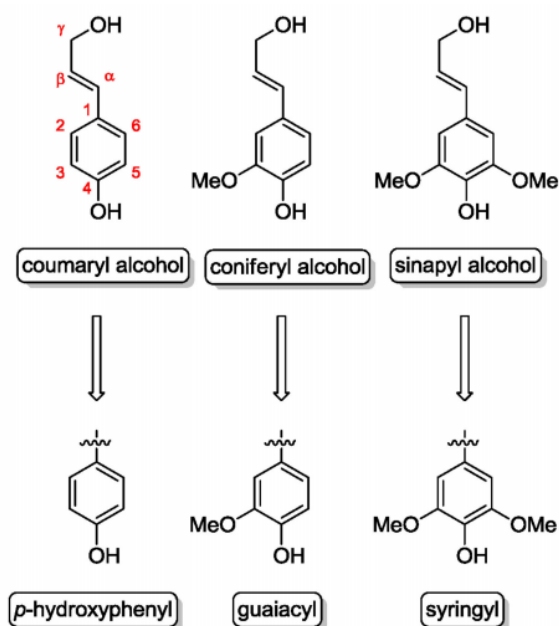
Figure 1.2: Monolignol units and the resulting building blocks present in lignin.[13]

Lignin plays an important role as a plant component. It provides the rigidity to cell plants and acts as a protective barrier of woody tissues against microbial and fungal attack[15]. Also, unlike polysaccharides that are hydrophilic, lignin is hydrophobic, so it allows water fluid, by repelling water. Besides, lignin decomposes slower than cellulose and the hemicellulose, in a range from 200 °C to 500 °C,[16] and its density is reported around 1395 kg/m^3.[17]

1.1.2 Lignin Properties

Lignin has features and properties which depends on its structure. The main properties are briefly explained below:

Antioxidant properties: Lignin is characterized by its antioxidant properties, by virtue of its structure that shows free radical scavenging ability.[18] Lignin acts as antioxidant by exerting activities such as hydrogen atom transfer and single electron transfer determined by the presence of free phenolic hydroxyl groups and substitution in the ortho position by methoxy groups in aromatic rings.[19] The presence of hydroxyl groups makes lignin a polar polymer, so it will not be very soluble in nonpolar media which may restrict its reactivity with the free radicals that cause oxidation.[20]

UV absorption property: In wood, analyses have shown that approximately 80-95% of the incident light is absorbed.[21] Thus, lignin stands out for its UV absorption ability. Its property is attributed to the content of chromophores, i.e. UV-Vis absorbing groups. These chromophores include ring-conjugated ethylenic groups such as cinnamaldehyde structures as well as carbonyl groups such as α-carbonyl groups and quinones[22].

Antimicrobial properties: Lignin has shown good performance as an antimicrobial agent. Studies have shown that the antimicrobial ability in lignin corresponds to the presence of phenolic compounds[23].

Other properties such as antifungal and antiparasitic[14] have been reported. Moreover,

lignin is a polymer with a high thermal stability and exhibits environment-friendly and biodegradable benefits. All these abilities make lignin an excellent source for materials development.

1.1.3 Extraction methods for lignin

The isolation of lignin in its native form is very difficult since the methods applied to cleavage of lignin–carbohydrate linkages cause alterations in the structure of lignin[24], i.e. the structure of isolated lignin depends on its native origin and separation process. Some of the known treatments for the extraction and isolation of lignin are alkaline, acidic, hydrothermal, wet oxidation and organosolv methods.[25] Studies have shown that lignin obtained from organosolv treatment has a high purity and homogeneity than lignins obtained from other treatments.[26] Therefore, it is a very suitable alternative for the fractionation of lignocellulosic components, despite its expensive cost. Organosolv method is based on the extraction of lignocellulosic biomass with a mixture of organic solvents and water. The most used solvents in this treatment include methanol, ethanol, propanol, butanol, benzyl alcohol, glycerol, glycol, acetone, formic acid, acetic acid, propionic acid, among others.[27]

In the organosolv treatment, delignification is produced by the cleavage of ether bonds by H^+ ions. The α-aryl-ether and β-aryl-ether are hydrolized, being these last bonds, harder to break.[28] The cleavage of β-O-4-aryl ether linkage is important for degradation of lignin structure since it represents about 50% of the ether linkages in lignin,[29] this linkage is represented in the Figure 1.3. The cleavage of β-aryl-ether bond leads to free phenolic groups and Hibbert ketones (keto-containing structures)as indicated by the mechanism in the Figure 1.4.
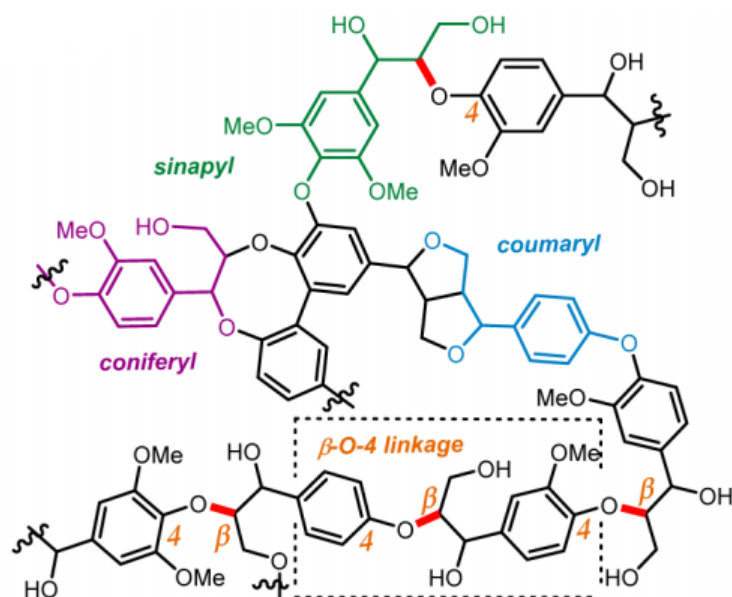
Figure 1.3: Representative scheme of a lignin molecule and β-O-4 bond.[30,31]
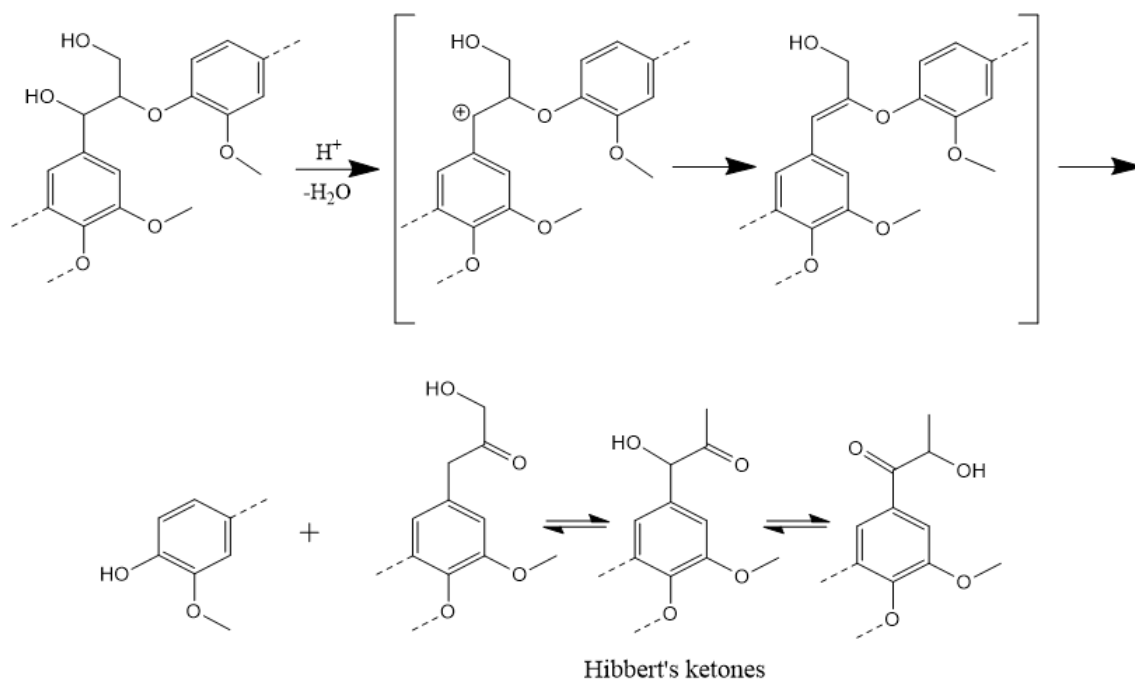
Figure 1.4: Acid-catalyzed cleavage of the β-aryl ether bond.[32,33]

Literature reports that acetic acid has proved to be an efficient solvent to fractionate lignocellulosic materials and for the delignification of wood.[34] Besides, acetic acid-based

pulping processes have aroused a recent interest due to its low environmental impact. Acetic acid delignification may be enhanced by adding some amounts of formic acid because formic acid (pKa 3.7) is stronger than acetic acid (pKa 4.8).[35,36] Formic acid is a selective solvent for the cleavage of the lignin β-O-4 bond[1]. Therefore, the main lignocellulosic components can be separated by acetic acid combined with formic acid. After organosolv treatment, lignin and hemicelluloses are dissolved in the solvent and cellulose remains solid.

Millions of tons of biomass waste are produced every year around the world. Most of these products are usually disposed of in landfills, creating damage associated with pollution. Lignocellulosic waste is also usually burned emitting a large number of greenhouse gases. This occurs mainly in countries that lack a controlled burn policy. For these reasons, a large number of studies are currently carried out to take advantage of these wastes and create value-added products.[37,38]

1.2 Biomass in Ecuador

Ecuador is located on the west coast of South America. It has an area of 283.560 km^2 and is divided into four distinct geographic regions: Coastal Lowlands, Andean Highlands, Amazon Rainforest and Galapagos Islands. The climate varies by region and altitude. This country is benefited from its geographical location, and climatic conditions, which allows its agricultural wealth and harvesting a diverse range of high-quality products. Ecuador is a recognized agricultural producer, being the principal agricultural products bananas, coffee, cocoa, flowers, corn, rice husks, potatoes, among others.

Ecuador is the third-largest supplier of flowers in the world market, behind the Netherlands and Colombia. Around 73% of the total flowers exported correspond to roses. It is estimated that there are over 400 varieties of roses in this country. The main rose production is concentrated in the northern highland region, in cities such as Cayambe, Tabacundo and Otavalo where temperatures ranging from 10 °C to 20 °C offer

the most suitable conditions for the production of roses. Also, Ecuadorian flowers have certain characteristics like a variety of colors, larger and thicker stems, and durability, which makes them one of the favorites worldwide. According to data from ESPAC, a survey conducted by the Institute of Statistics and Censuses of Ecuador (INEC) in 2018, the area planted with roses was 4,966 hectares, which represents 66.1% of the national total of cultivated flowers. The rose stands out as the flower with the highest production with 3.199 million cut stems[39].

As regards corn, it is one of the main export products from Ecuador. During 2018, the area destined for the sowing of temporary crops was 941,280 hectares, the main crops corresponded to rice, corn, and potatoes. Corn accounted for 40.7% of the total area planted with temporary crops. Its largest production was mainly concentrated in coastal provinces such as Los Ríos (38.8%), Manabí (24.9%) and Guayas (17.5%).[39] Temporary crops refer to crops characterized by growth in less than one year. In the Figure 1.5 is represented the main producing Ecuadorian provinces of the two crops that are of interest in this research are represented.
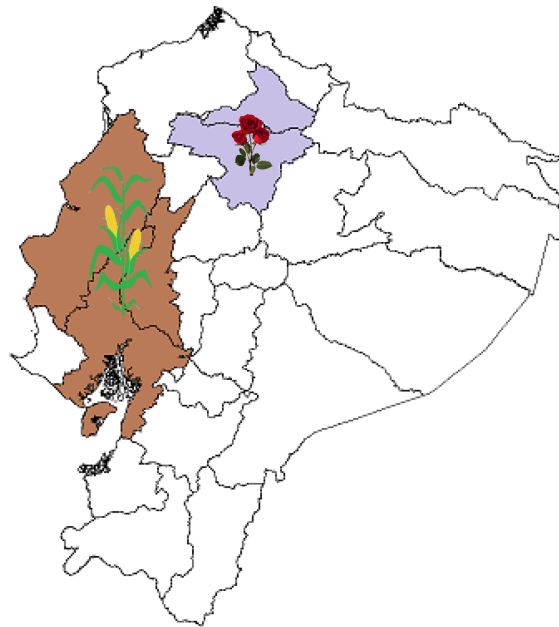
Figure 1.5: Political map of Ecuador and producing provinces of rose (purple color) and corn (brown color).[40]

As evidenced, Ecuador has a large abundance of biomass as a result of agricultural activities and natural forests. However, biomass is usually discarded and underestimated by the lack of alternatives and technologies to make the best from it. In addition, Ecuador receives a large amount of solar radiation as a result of its location. The cities of the Andean region are located at very high altitudes above 2000 meters above sea level, where solar radiation intensifies.

1.3   Sun exposure

Electromagnetic radiation consists of the flow of photons propagating in space. There are different types of radiation depending on the energy of the photons. It includes radio waves, microwaves, infrared waves, visible light, ultraviolet radiation, X-rays, and gamma rays, ranging from low energy to high energy.

The UV radiation in small amounts is beneficial to health by stimulating the production of vitamin D and endorphins in the skin. However, higher sunlight expositions are harmful to human health[41] and organic materials[42]. The main source of energy is sunlight. The amount of solar energy on a surface area is quantified by solar irradiation, it is expressed in watt per square meter (W/m^2) unit.

Currently, there are higher levels of UV radiation reaching the Earth's surface as a result of ozone layer depletion. The sun emits ultraviolet radiation that covers a wavelength region from 100 nm to 400nm. UV radiation is divided into three types which are UVA (320–400 nm), UVB (290–320 nm), and UVC (100–290 nm). The longer wavelengths have lower energy, and therefore, less harmful. In contrast, a shorter wavelength is the most damaging radiation type. UVC is a short wavelength radiation and the most harmful. However, this type of radiation is completely absorbed by the ozone layer and does not reach the atmospheric surface.[43] UVB has a medium wavelength, it has been reported that this radiation causes important biological effects as human skin burning. Most UVB radiation is filtered by the ozone layer. UVA has the longest wavelength

radiation. This radiation represents approximately 95% of the total UV radiation that reaches the earth.[44] Although UVA rays are less intense than UVB rays, they cause long-term damage to the skin. Figure 1.6 illustrates the penetration of different UV rays wavelengths.
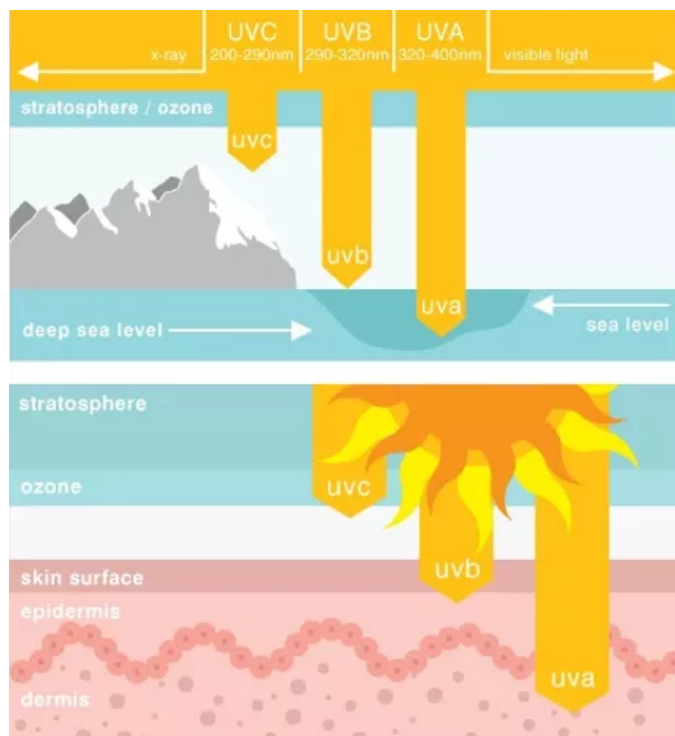
Figure 1.6: Representation of UV radiation.[45]

As mentioned before, UVA and UVB cause severe human skin damage. Long time to solar radiation exposure can lead to problems like the aging of the skin, the presence of wrinkles, eyes damages as cataracts and eyelid cancers, and genetic defects by DNA cell damage.[44]. For skin protection, sunscreens are useful to avoid the adverse effects of solar radiation. The use of sunscreens should be done daily to avoid having premature sking aging and other future problems such as cancer. Chemically, sunscreens are composed of UV absorbers. Titanium oxide (TiO_2) and zinc oxide (ZnO) are the most used compounds as inorganic sun blockers. These two oxides are usually combined to provide broad-band UV protection due to TiO_2 is a potent absorber in UVB and ZnO in UVA range.[46] However, synthetic

chemicals can cause side effects when used for long periods,[47] so natural materials such as lignin can be used as a possible sunscreen.

Besides, photo-degradation is another problem derived from sunlight. It causes the degradation of organic compounds by absorbing photons which lead of breaking of chemical bonds undergoing degradation reactions.[48] Some of the problems associated with UV radiation are discoloration of dyes and pigments, weathering, yellowing of plastics, loss of mechanical properties and other damages.[47] Therefore, it is necessary to protecting us and the affected organic materials against sunlight radiation. Inorganic UV absorbers as titanium dioxides and cerium oxide; and organic stabilizers with UV-absorbing properties such as green coffee and lignin[42], are employed for protection of organic materials as PVA. These products are of great interest in many different applications in cosmetic, textile and polymeric industries, for enhancing products able to remain unaltered by UV exposition for long periods of time.

1.3.1 Polyvinyl Alcohol (PVA)

PVA has been widely studied for the production of blend films with enhanced properties. Its chemical formula is $(C_2H_4O)_n$, where n indicates the repeating unit of a polymer chain. Vinyl acetate molecules (ethenyl ethanoate) linked through carbon-carbon bonds are polymerized to polyvinyl acetate and then hydrolyzed, getting PVA. Its molecular structure is given in Figure 1.7. PVA exhibits different molecular weights and hydrolysis degree. It is a synthetic, non-toxic, hydrophilic, biocompatible and biodegradable polymer.[49] PVA displays multiple properties such as chemical and thermal stability, high tensile strength, and oxygen barrier properties, that make it better over other polymers.[50] Besides, its exceptional characteristic of hydrophilicity allows it to be a suitable polymer for being used in the production of composite films.
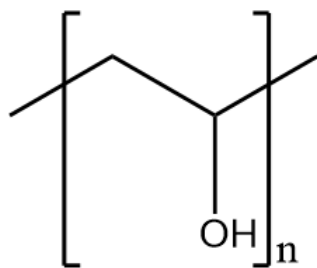
Figure 1.7: Structure of polyvinyl alcohol (PVA).

CHAPTER 2

PROBLEM STATEMENT

Ecuador is a country rich in the production of different sorts of plants. However, most of the residues from agricultural harvesting as stems, leaves, bagasse, stalks, branches, husk, among other biomass products, are discarded without being taken advantage of. In order to produce value-added products from biomass, the extraction of lignin, one of the main polymeric constituents of these agricultural biomass residues is proposed. Lignin is a promising alternative as raw material due to its low-cost, renewable source, high availability and great properties as UV-absorption ability.[37] Recently, the use of natural products for radiation protection has received a special interest since it has been shown that the use of synthetic chemicals can cause adverse effects.

In this work, it is intended the extraction of lignin from two different biomass source, followed of their respective characterization. Then, a possible application of lignin is carried out as a great alternative for replacing synthetic chemicals from UV absorbers.

CHAPTER 3

OBJECTIVES

3.1 General Objective

- Harnessing of sources obtained from agricultural waste such as rose stems and corn stalks for the preparation of high added value materials.

3.2 Specific Objectives

- Extraction of lignin from lignocellulosic biomass (rose stem and corn stalk) by an organosolv treatment for obtention of micro/nano lignin particles.

- Characterization of lignin particles by different physico-chemical techniques, such as Infrared Spectroscopy (IR), Scanning electron microscope (SEM), Energy-Dispersive X-Ray (EDX) Spectroscopy, Dynamic Light Scattering (DLS), Zeta Potential, UV-VIS spectroscopy, and X-ray diffraction analysis (XRD).

- Design and evaluation the UV absorption ability of lignin particles through the preparation of PVA-lignin films.

CHAPTER 4

METHODOLOGY

4.1 Reagents

Rose stems and corn stalks were obtained from agricultural wastes in Imbabura Province for lignin extraction.

Glacial acetic acid was purchased from Novachem (Australia), 98% formic acid was obtained from Loba Chemie Laboratory (India), glacial sulfuric acid 95-97% was supplied by Sigma -Aldrich (USA) and sodium hydroxide Emsure (Germany). Finally, for the production of films, Polyvinyl Alcohol (PVA), with a degree of polymerization of 1700-1800, was purchased from Loba Chemie Laboratory (India).

4.2 Materials

Table 4.1: Materials and devices used during the experimental process

Materials		Equipment	Analytical Instruments
Beakers	Soxhlet Equipment	Grinder	Scanning Electron Microscope + EDX detector
Kitasate	Buchner funnel	Magnetic stirrer hot plate	FTIR spectrometer
Filter paper	Threaded bottles	Rotary evaporator	DLS/Zeta Potential analyzer
Round flask	Gooch Crucible	Autoclave	UV-Vis spectrophotometer
Test tubes	Erlenmeyer flasks	pH meter	X-ray diffractometer
Stirring Rods	Magnetic stir bar	Balance	Digital UV light meter
Plastic petri dishes	Eppendorf tubes	Shaking water bath	
Shaking water bath	Vials	Oven	
		Stirring water bath	

4.3 Experimental procedure

4.3.1 Process of lignin extraction

The method followed for lignin extraction was an acidic treatment proposed in the literature[51]. Figure 4.1 depicts a flow chart of the proposed procedure, which consisted in:

- Rose stems and corn stalks were washed, cut in small pieces and finally milled by using an electric coffee grinder.

Biomass

Rose stems

Corn stalks

cellulose

85% organic acid (ratio of formic acid/acetic acid mixture was 70:30 by volumen)

lignin liquors

Liquid was heated at 105°C and distilled water was added (5 times more than volume)

solid

ICL1
IRL1

CL-1
RL-1

Liquid was concentrated by rotoevaporation at 75°C and then, stored

Filter the recovered product and wash it with 80% formic acid followed by hot distilled water.

Figure 4.1: Scheme of experimental procedure for lignin extraction from rose stems and corn stalks.

- 10-g amount of each sample was put into a Soxhlet apparatus with a mixture of 85% organic acid (ratio of formic acid/acetic acid mixture was 70:30 by volume) for 4h in order to extract lignin liquors delignifying lignocellulosic material. Once this time was over, the resulting cellulose in the solid pulp was stored while the obtained liquors were heated at 105 °C.

- Distilled water was added to liquors in a ratio of 1:5 (five times more than liquors volume) to precipitate the lignin dissolved in acetic and formic acid.[1].

- The precipitated formed was subjected to a vacuum extraction on a Buchner funnel using a filter paper with a pore size of $1 - 2\,\mu$m. The remaining solid samples were washed with 80% formic acid and distilled sample. Once dried, ICL1 and IRL1 samples were stored for further analyses.

- Filtrate was concentrated by using a rotary evaporator equipped with a V-300 vacuum pump (Büchi Labortechnik) at 75 °C. The remaining lignin of both corn and rose was concentrated while the solvent with the hemicellulose sugars and other components were removed.

- These tiny and alkali-soluble lignin samples were collected and washed successively with water, obtaining the samples CL-1 and RL-1, corresponding to corn lignin and rose lignin of tiny size, respectively. These samples were stored in vials for further chemical analyses.

4.3.2   Acid Hydrolysis for determination of Klason Lignin

This following procedure was carried out as provided by NREL Laboratory Analytical Procedures[52], which consisted in:

- A known amount of the crude lignin samples (previously extracted) was dried in an oven for 12 hours.

- The solid samples were placed in test tubes, and H_2SO_4 (72% by weight) was added in a ratio of 0.1: 1 (gr/ ml). Then, the test tubes were placed in a shaking water bath for 1 hour at 30 °C. The samples were stirred with the stirring rod every 5 to 10 minutes to ensure contact between sulfuric acid and lignin particles and the uniform hydrolysis process.

- The contents of the test tubes were transferred to the threaded bottles. To collect all the adhered material from the test tubes, each tube was washed with 40 ml of deionized water to dilute the acid.

- Solution was poured into the bottle and 100 ml more water was added to the threaded bottles of the autoclave.

- Samples were exposed at 121 °C for 60 minutes in an autoclave. Once the process was finished, the autoclave was allowed to cool to room temperature and the bottles were removed.

- The bottles with their content were weighed again and then, the content was filtered on Gooch crucible (previously dried in the oven and weighed).

- The crucible and contents were dried in the oven at 100 °C overnight and weighed to obtain the purified lignin.

- Finally, the amount of the acid insoluble lignin (AIL) was determined by the following expression:

$$\%(AIL) = \frac{W_{cds} - W_{dc}}{W_{ds}} \times (100) \tag{4.1}$$

where $\%(AIL)$ is the amount of acid insoluble lignin, W_{cds} is the weight of the crucible with dry sample, W_{dc} is the weight of the empty dry crucible, and W_{ds} the weight of the dry sample.

4.3.3 Preparation of PVA-lignin films

PVA films with different lignin concentrations were prepared by dissolving polyvinyl alcohol in distilled water in a beaker by heating in a hot plate at 150 °C with continuous mixing until the solution was homogeneous. Then, they were added different volume concentrations (0.5%, 1%, 2% and 4%) of lignin to the soluble PVA while stirring until the lignin was dispersed in the solution. Also, a solution with only PVA was prepared for being used as a reference. Films were prepared by pouring the solution onto plastic Petri dishes of 5 cm of diameter, and the plates were left to dry into an oven at about 40 °C for 20 h. Images of the dried films are shown in Figure 4.2.
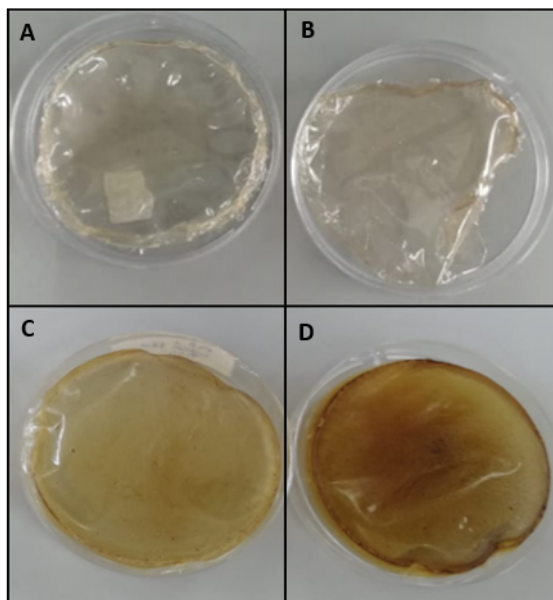
Figure 4.2: PVA+ 0.5% lignin (A), PVA+ 1% lignin (B), PVA+ 2% lignin (C) and PVA + 4% lignin (D)

Evaluation of UV skin protection was carried out by using four samples . These samples included two commercial sunscreens, a moisturizer with and without lignin. Sunscreens were Umbrella 100 SPF, and Bioderma 50 SPF. Pure cream was NIVEA soft moisturizing cream and to this was added the low lignin content. Samples were tested using glass slides and subjecting them to solar radiation, and UV radiation from lamp.

4.3.4 Characterization of lignin and lignin-based materials

In order to characterize the obtained lignin and lignin-based materials from corn and rose stems, some analytical techniques were carried out.

FTIR measurements were done on Bruker iFS 66VS spectrometer, from 4500 to 300 cm^{-1}, at 2 cm^{-1} resolution. The powder samples were prepared by the standard method for the FTIR spectrometer using KBr. Approximately 2 mg of the samples and 200 mg of KBr were used. The sample was ground until a fine powder was obtained, which was then uniformly mixed with dry KBr powder. Using a hydraulic press, the sample mixture was

pressed to form a pellet. This analysis was performed by the IR technical manager of the Institute of Materials Science of Madrid.

Morphology studies were examined by field emission Scanning Electron Microscope using a FEI Nova NanoSEM 230 microscope equipped with a detector EDAX Genesis XM2i for EDX signals. The samples were dried at room temperature for 2 days. Also, for analyses, samples were deposited into the conductive carbon adhesive tapes.

Dynamic Light Scattering (DLS) and Zeta Potential measurements were developed by using Brookhaven Instruments PALS Zeta Potential Analyzer (Brookhaven Instruments Corp.). The pH values of samples were adjusted to 3, 5, 7 and 9 by the addition of sodium hydroxide (NaOH) by using a shaker at 27 °C and 50 rpm. Then, concentrated samples were diluted with distilled water. To homogenize the dispersion of particles in the sample, it was placed for 5 min in an ultrasonic bath. For both techniques, two measurements of each sample were collected to ensure its reproducibility. Also, each measurement consisted of 3 runs with 3 min. duration per run.

DLS provided information about effective diameter, mean distribution by number and polydispersity. Effective diameter (D_m) represents an average diameter weighted by the intensity of light scattered by each particle.[53]. Multimodal size distribution by number offers information about the size range of particles, that is to say, information regarding the groups of particles of different sizes, and polydispersity index (PDI) allows to know if the distribution of the particles is uniform.[54] The PDI values range from 0 (for homogeneous samples with respect of particle size) to 1.0 (for samples with heterogeneous particle size populations).[55]

Zeta potential measurements were collected by using the Phase Analysis Light Scattering (PALS) method which has very good sensitivity and estimates the electrophoretic mobility of particles by measuring their motion in an applied electric field.

Optical measurements were performed using a UV-Vis recording spectrophotometer

(Shimadzu UV-2401PC) with a dual-beam measurement. Samples were highly diluted in distilled water and poured into a quartz glass.

X-ray diffraction was performed for lignin powder samples through a Bruker D8-Advance DaVinci diffractometer using Cu Kα radiation (λ = 1.542 Å). The samples were finely ground using a mortar and pestle. Scans were done in the 2θ range from 0 ° to 50 °.

UV transmittance of the PVA-lignin films was measured. In this experiment, the PVA-lignin films were exposed to natural sunlight and the radiation that passed through the films was recorded by using a digital light meter model UV513AV which measures UV radiation in a spectral range of 280 to 400 nm.

Finally, for evaluating the stability of the UV protection of the films, a chamber was prepared with a UV lamp as a light source with the following features: 25W, 110V and a wavelength around 185nm, corresponding to UVC radiation. This potential light source was used to drive the photodegradation process of films and study the stability of the films even under UVC range.

Information associated with each one of these characterization techniques is given below.

4.3.5   Fourier-transform infrared spectroscopy (FTIR):

Infrared spectroscopy is an important tool for the identification of functional groups present in molecules since molecules absorb specific frequencies that are characteristic of their structure. When molecules absorb infrared radiation, its chemical bonds vibrate and the molecules are excited from a ground state to an excited vibrational state. The bond of a molecule experiences molecular vibrations which are of two types: stretching that changes the bond length and bending that changes the bond angle. For the determination of functional groups, molecules must have a dipole moment that changes as a function of time. When the infrared radiation interacts with the covalent bond of the materials having an electric dipole, the molecule absorbed energy, and the bond

starts back and forth oscillation. Thus, the oscillation that causes the change in the net dipole moment of the molecule, absorb infrared radiations.
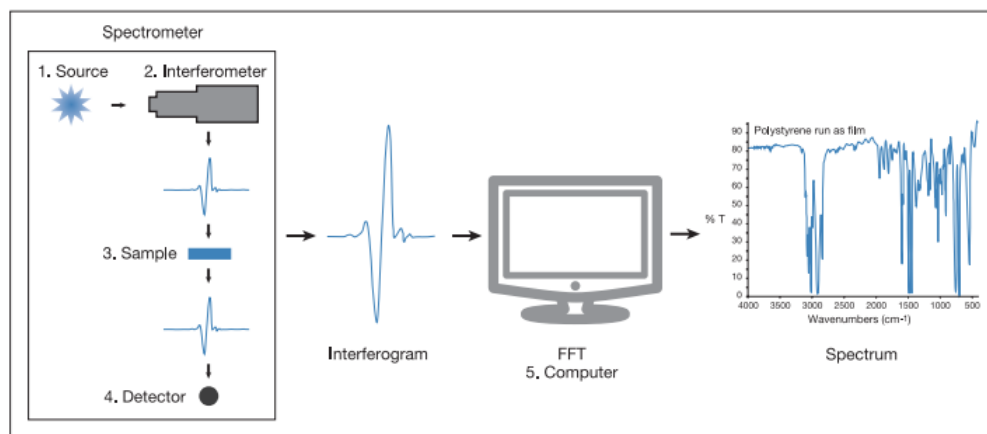
Figure 4.3: Schematic diagram of FT-IR system.[56]

The prepared sample is placed into a pellet holder and positioned in the spectrometer as the Figure 4.3 indicates. Then, infrared radiation passes through the sample, and some radiation is absorbed by the sample while the other fraction is transmitted. The resulting signal is digitized and sent to the computer giving a plot of absorption of infrared radiation by the sample material versus wavelength of light.

For spectral interpretation, it is necessary to identify the 2 regions of a spectrum which are 1) functional group region (from about 4000 to 1500 cm^{-1}) that shows characteristics peaks of specific bonds and 2) the fingerprint region in the right-hand side of the plot (from about 1500 to 400 cm^{-1}) which provides particular information for each molecule. Also, infrared correlation tables are very useful to identify the frequencies at which various functional groups absorb and they are easily found in the literature.

4.3.6   Field Emission Scanning Electron Microscopy (FE-SEM) and Energy-Dispersive X-ray (EDX) Spectroscopy

SEM and EDX analysis are two excellent techniques that combined form a powerful tool for determining particle sizes and elemental composition of materials, respectively.

SEM is a technique widely used for surface characterization of materials, based on the production of images by scanning the sample with a high-energy beam of electrons. Unlike optical microscopes use visible light, electronic microscopes use electrons for imaging. Since the wavelength of electrons is much smaller than the wavelength of visible light, the resolution of SEM is much better providing detailed topography information as size and shape.[57]

A schematic representation of the SEM instrument is shown in Figure 4.4. Electrons are generated at the top of a column by the source of electrons. The entire column must be under vacuum and the electron source inside a chamber to be protected from noise and contamination. Usually, samples are dried preventing any disturbing contamination, and then mounted on the holders using double-sided conductive tapes as carbon tapes providing excellent adhesion and conductivity to samples. These samples are located in the specimen holder inside the chamber area where the electron beam passes through a series of condenser lenses and apertures to hit and penetrate the sample to a depth of a few microns. The depth will depend on the applied voltage and the density of the sample.[58] As a result of the electron-sample interaction, several signals are produced and collected by detectors, forming a three-dimensional image of the surface topography of samples.

Moreover, Energy-Dispersive X-ray (EDX) Spectroscopy is a qualitative and quantitative analysis that provides information on the different types of elements present in the sample and the concentration of each element.[60] As the focused beam of electrons of the SEM is emitted across the sample surface, it produces specific wavelengths X-rays which are
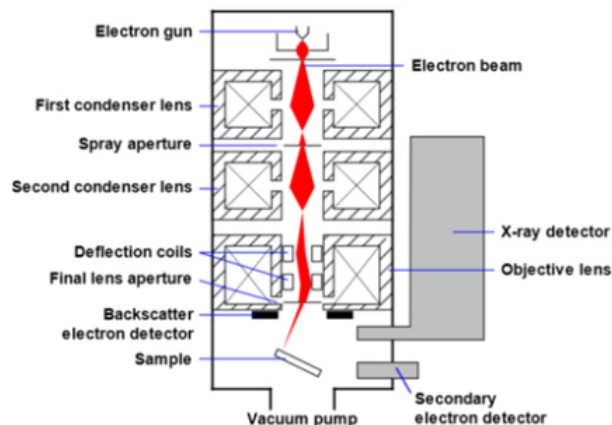
Figure 4.4: Schematic diagram of a Scanning Electron Microscope.[59]

characteristics of each element. The depth from where the X-rays originate will depend on the primary electron beam energy and the nature of the material. The detectors are responsible for detecting the X-rays and giving elementary information about the sample. The information about the heights of specific peaks are compared with known materials to obtain a quantitative analysis of sample composition.

4.3.7 Dynamic light scattering (DLS)

It is an ideal technique used to determine the size of the particles through the study of the random movement of particles in solutions. In this analysis, the particles are illuminated with a laser beam, and the fluctuations of the scattered light, as a result of the speed of Brownian motion of particles, are detected. The rate of fluctuations is strongly dependent on the size of the particles. The larger the particle, the slower the Brownian movement and the smaller, move faster[61]. The rate of the Brownian motion is known as the translational diffusion coefficient and it is calculated using the Stokes-Einstein equation as follows:

$$d(H) = \frac{kT}{3\pi\eta D} \tag{4.2}$$

where $d(H)$ is the hydrodynamic diameter, D is the translational diffusion coefficient, k is the Boltzmann constant, T is the absolute temperature, and η is the viscosity.

This previous equation assumes that the particles are spherical and that the concentrations are low[62]. Moreover, it is essential to have a stable temperature to know the viscosity and avoid random movements of the particles.

For this procedure, samples are poured into the cells, where a laser beam passes through it. A detector is responsible for noticing the intensity fluctuations of scattered light.

4.3.8   Zeta Potential

Zeta Potential Measurement allows knowing the electric charge at the interface between solid particles and a liquid medium. The surface charge affects nearby ions leading to the formation of a non-uniform electric charge distribution near the interface called electric double-layer[63]. Zeta potential data is a very useful technique to know the physical stability of suspensions.

Figure 4.5 shows the electrical double layer which is a model that explains the net electric surface charge. The liquid layer surrounding the particle exists as a Stern layer or inner region which is charged opposite to the surface charge and therefore strongly bound, and an outer region known as the diffuse layer containing free ions where they are less firmly associated.[64] In the diffuse layer, ions and particles form a stable entity. When a particle moves (e.g. due to gravity), ions within the boundary move it. Those ions beyond the boundary stay with the bulk dispersant. The potential at this boundary (surface of hydrodynamic shear) is the Zeta potential.

The stability of a colloidal system is given by the magnitude of the Zeta potential while the sign shows the dominant charge at the surface, either positive or negative. It is normally considered that particles with Zeta potentials more positive than +30 mV or more negative than -30 mV are stable. Particles with a very low Zeta potential absolute value can lead to agglomeration and flocculation because there are not forces to prevent it while the particles with a large Zeta potential value tend to repel each other and be

separated. One of the factors that most affect the Zeta potential is pH, H^+ can cause the buildup of positive charge on a particle's surface while OH^- will add negative charge thus altering the Zeta potential.[65] Also, functional groups at the particle surface may become protonated/deprotonated.
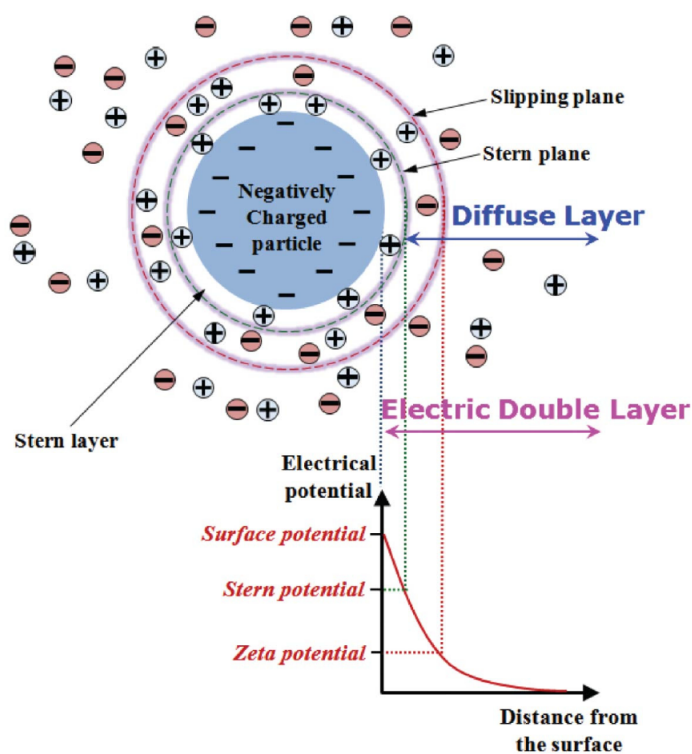
Figure 4.5: Schematic representation of electric double layer.[66]

The process consists of placing the sample solution in a cell that contains two electrodes, a laser light is applied which passes through the center of the sample cell. When the electric field is applied, the particles contained in the volume will cause the intensity of the detected light to fluctuate with a frequency proportional to the particle speed, the information is identified by a detector.[67]

4.3.9   Ultraviolet–visible spectroscopy (UV-Vis)

It is a technique widely used for the characterization of materials. It allows determining the optical properties such as absorbance, transmittance, and reflectance of liquids and solids. The concentration of an analyte in a solution can be determined by measuring the absorbance at a particular wavelength through the Beer-Lambert Law. UV spectrometer is capable of scanning the wavelength range 200-400 nm and the visible region 400-800 nm. Chemically, molecules in the sample undergo some state transition from a lower to a higher state.[68]

According to Beer-Lambert Law, absorbance of the sample solutions is directly proportional to the concentration of the medium and the length of the light path, as follows:

$$A = \varepsilon c l = log\frac{I_o}{I} \tag{4.3}$$

where A is the absorbance, ε is the molar absorptivity for determined compounds at specific wavelength, c is the concentration of absorbing sample, l is the length of the cell, I_o is the intensity of the incident light and I is the intensity of the transmitted light through the sample.

For optical measurements, the sample solution is placed into a cuvette which is typically made of glass or quartz, which usually has a path length l given in centimeters. A beam of light from a visible light source (usually tungsten lamps) or UV light (halogen or deuterium lamps) is separated by a prism or diffraction grating which breaks down light into its constituent wavelengths. Then, each monochromatic beam is divided into two beams of equal intensity using a beam splitter. The resulting beams pass through the reference cell and the sample cell as is indicated in Figure 4.6. The intensities of these beams are measured by detectors and a plot of absorbance vs wavelength is obtained by data processing. Depending on the optical properties of the sample solution, fractions of the monochromatic beam can be absorbed, transmitted or reflected.
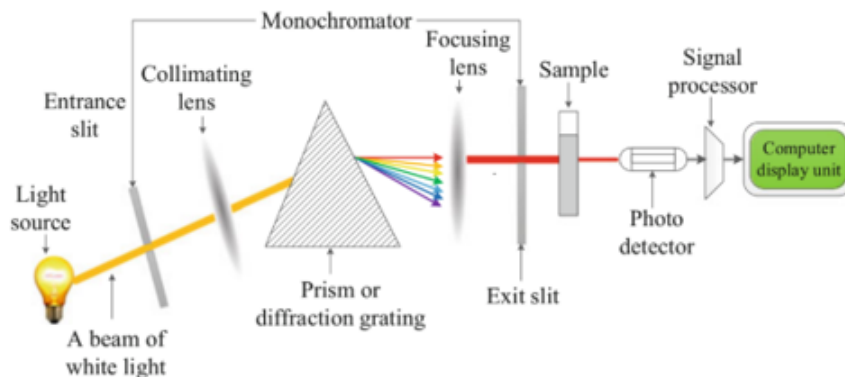
Figure 4.6: Schematic diagram of a double beam UV-Visible Spectrometer.[69]

4.3.10 X-ray Diffraction Analysis (XRD)

By XRD, a qualitative and quantitative analysis of unknown crystalline materials can be achieved. This technique provides information on the crystalline structure, degree of crystallinity and crystalline phases present in a sample. Besides, it allows studying amorphous materials, as is the case of lignin, where it is only possible to find a halo diffraction.[70]. This technique is based on Bragg's law (Equation 4.4) where constructive interference which is caused by the interaction of the sample with X-rays, produces a diffraction pattern.[71].

$$n \, \lambda = 2 \, d \, sin\theta \tag{4.4}$$

where n is the integer, λ is the wavelength of the incident X-rays, d is the interplanar spacing of the crystal and θ the angle between the incident beam and the normal to the reflecting lattice plane. During this procedure, the sample is bombarded by a monochromatic beam of X-rays, the scattered X-rays interfere with each other undergo constructive interference, which are recorded in a detector.

CHAPTER 5

RESULTS

An organosolv treatment was carried out for the extraction of lignin from two agricultural biomass residues. As was previously mentioned, rose stems and corn stalks were refluxed with a mixture of formic acid, acetic acid, and distilled water. Lignin was expected to dissolve in the organic acid solvents due to their ether bonds- cleavage, and the hemicellulose is degraded into sugars (mono and oligosaccharides), and the solid residue is the cellulose. Then, when adding water to the concentrated spent liquor, water-insoluble lignin particles precipitated. After, filtration was carried out to separate the greater size particles lignin from other lignin sub-micrometric particles. This part of the procedure was carried out successfully for the biomass corn, obtaining insoluble corn lignin (ICL1) with a size larger than $1-2\,\mu$m. However for the biomass of the rose, only a small amount of insoluble rose lignin (IRL1) was obtained, while most lignin content passed directly to the filtrate phase as a result of their small size $(< 1-2\,\mu$m). By a rotary evaporation process the remaining lignin in the filtrate phase was concentrated, removing solvents along with other species, such as those from hemicellulose degradation. It had been reported that hemicellulose degrade at a much faster rate than lignin, between 200 and 300 °C.[72]

From the results from EDX measurements it could be observed the presence of certain elements in lignin samples, so the acid hydrolysis procedure was applied to purify the lignin. This procedure is very suitable for the fractionation of lignin from other components such as carbohydrates, ashes, among other extractives.[52] Also, through this procedure the obtained lignin fractionates into Klason lignin; which is the acid-insoluble portion, and acid-soluble lignin. The equation 4.1 was applied with the objective of obtaining the percentage of Klason lignin , and the result showed a yield of 79.30%

5.1 Analysis of corn and rose lignin samples by different characterization techniques

5.1.1 Fourier-transform infrared spectroscopy (FTIR)

Lignin is a polymeric network with a variety of functional groups that are analyzed below. The most characteristic peaks of lignin were found in the fingerprint region ($\sim$400-1500 cm^{-1}). FTIR peaks were assigned comparing with spectra reported in other studies[73–75]. The Table 5.1 summarizes the main IR peak frequencies of lignin[74,75].

Table 5.1: IR assignments of lignin[74,75]

Wavelength (cm^{-1})	Assignments
1714-1725	Stretching of C=O unconjugated to aromatic rings
1655	Stretching of C=O conjugated to aromatic rings
1594-1609	Aromatic ring vibrations and C=O stretching
1504-1515	Aromatic ring vibrations
1462-1464	C-H assymetric deformation in CH_3 and CH_2 groups
1421-1424	Aromatic ring vibrations
1320-1330	Syringyl nuclei (C–O stretching)
1270-1268	Guaiacyl nuclei (C–O stretching)
1216-1225	C–C, C–O, C=O stretching in G ring
1114-1125	Aromatic C-H in-plane deformation in the S rings
1030-1033	C-H in-plane deformation
913-929	Aromatic out-of-plane C-H deformation
833-834	Aromatic out-of-plane C-H deformation in syringyl units

5.1.1.1   Lignin extracted from corn stalks

Figure 5.1 shown the FTIR spectrum of the resulting corn lignin sample ICL1. The band at $1724 \, \text{cm}^{-1}$ is attributed to stretching of C=O bond unconjugated to aromatic rings, while the peak at $1655 \, \text{cm}^{-1}$ corresponds to stretching of C=O bond conjugated to aromatic rings. Absorption bands at $1604 \, \text{cm}^{-1}$, $1515 \, \text{cm}^{-1}$, and $1425 \, \text{cm}^{-1}$ are associated to typical aromatic ring vibrations. The peak at $1463 \, \text{cm}^{-1}$ corresponds to C-H assymetric deformation in methyl and methylene groups. A peak at $1329 \, \text{cm}^{-1}$ indicates the C-O stretching of syringyl (S) nuclei, $1126 \, \text{cm}^{-1}$ corresponds to aromatic C-H in-plane deformation, and $835 \, \text{cm}^{-1}$ for C-H out of plane bending of S units. These previous signals suggest a high content of syringyl (S) units in lignin structure[73]. However, other bands corresponding to guaiacyl units are also found, $1225 \, \text{cm}^{-1}$ is assigned for C–C, C–O, and C=O stretching in guaiacyl G ring, and $1034 \, \text{cm}^{-1}$ for C-H in-plane deformation in G units. Peak around $1160 \, \text{cm}^{-1}$ suggests the deformation C–H bonds on benzene rings. Finally, the broad band in the range of $3100\text{-}3600 \, \text{cm}^{-1}$ indicates the presence of hydroxyl groups, and the peak at $2851 \, \text{cm}^{-1}$ corresponds to C-H stretching vibrations in methylene, and the one at $2935 \, \text{cm}^{-1}$ for C-H stretching of methyl groups. These results showed that corn lignin is composed of units of syringyl, guaiacyl and hydroxyphenyl units with a greater amount of syringyl units.

5.1.1.2   Lignin extracted from rose stems

The spectrum of the IRL1 sample is shown in Figure 5.2. There is a broad band at $3425 \, \text{cm}^{-1}$, characteristic of hydroxyl groups. Bands at $2935 \, \text{cm}^{-1}$ and $2850 \, \text{cm}^{-1}$ indicate the C-H stretching of methyl and methylene groups, respectively. Then, in the fingerprint region, the peak at $1720 \, \text{cm}^{-1}$ shows the vibrations of C=O bond unconjugated to the aromatic ring, and at $1655 \, \text{cm}^{-1}$ suggests the stretching of C=O conjugated to aromatic rings. The peak at $1609 \, \text{cm}^{-1}$ is related to aromatic ring vibrations and C=O vibrations. Other aromatic ring vibrations, typical of lignin pattern are exhibited at $1515 \, \text{cm}^{-1}$ and
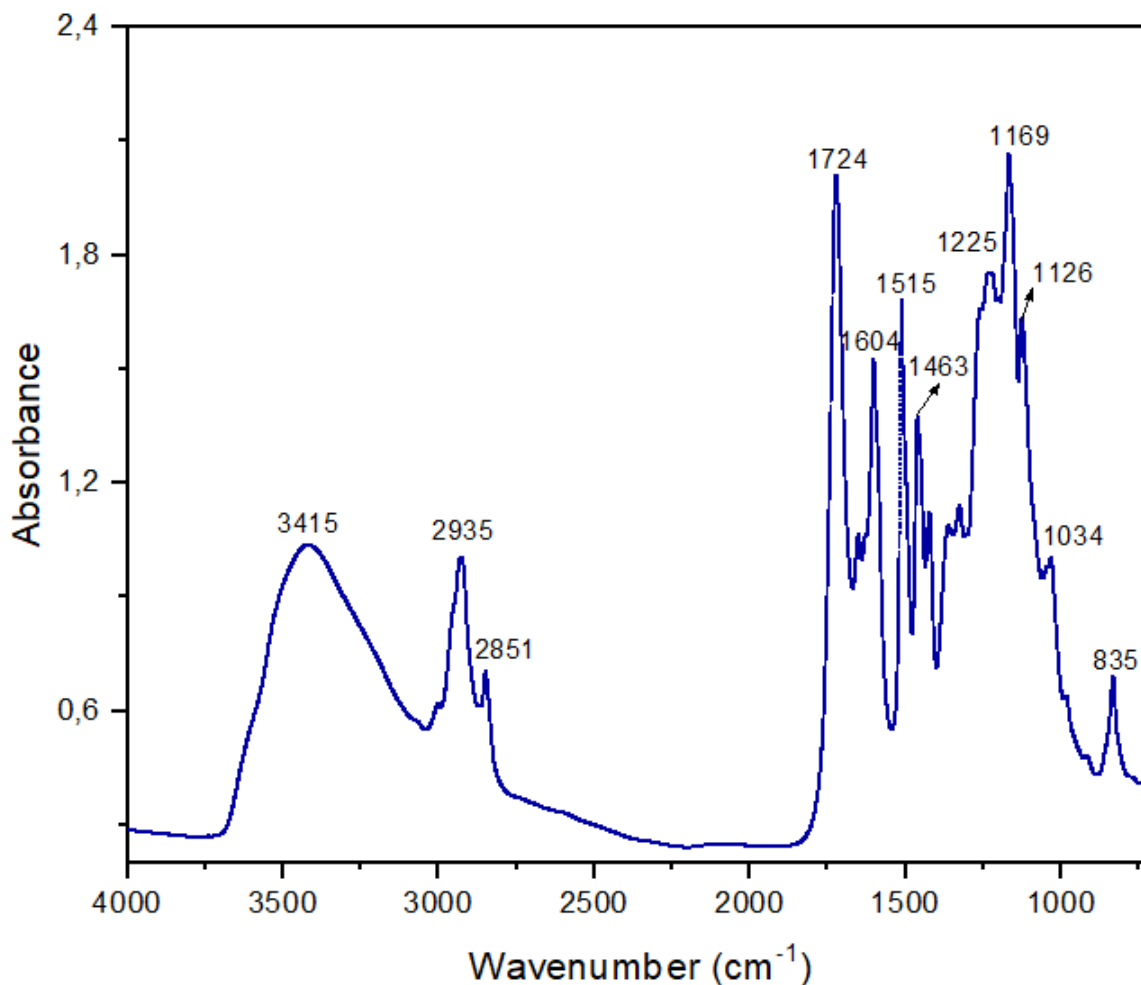
Figure 5.1: FTIR spectra for obtained corn lignin.

1424 cm^{-1}. Moreover, the band at 1464 cm^{-1} is assigned to C-H asymmetric deformation in CH_3 and CH_2 groups. The bands at 1328 cm^{-1} and 1269 cm^{-1} indicate the C-O stretching of syringyl (S) and guaiacyl (G) nuclei, respectively. C–C, C–O, and C=O stretching in guaiacyl (G) ring are designated at 1221 cm^{-1}. Vibrations at 1122 cm^{-1} corresponds to aromatic C-H in-plane bending, and that at 1033 cm^{-1} is associated to C-H deformation. Finally, the signal at 919 cm^{-1} indicates an aromatic out-of-plane C-H bending. With this analysis, the signals identified correspond to heterogeneous lignin with syringyl, guaiacyl, and p-hydroxyphenyl units.
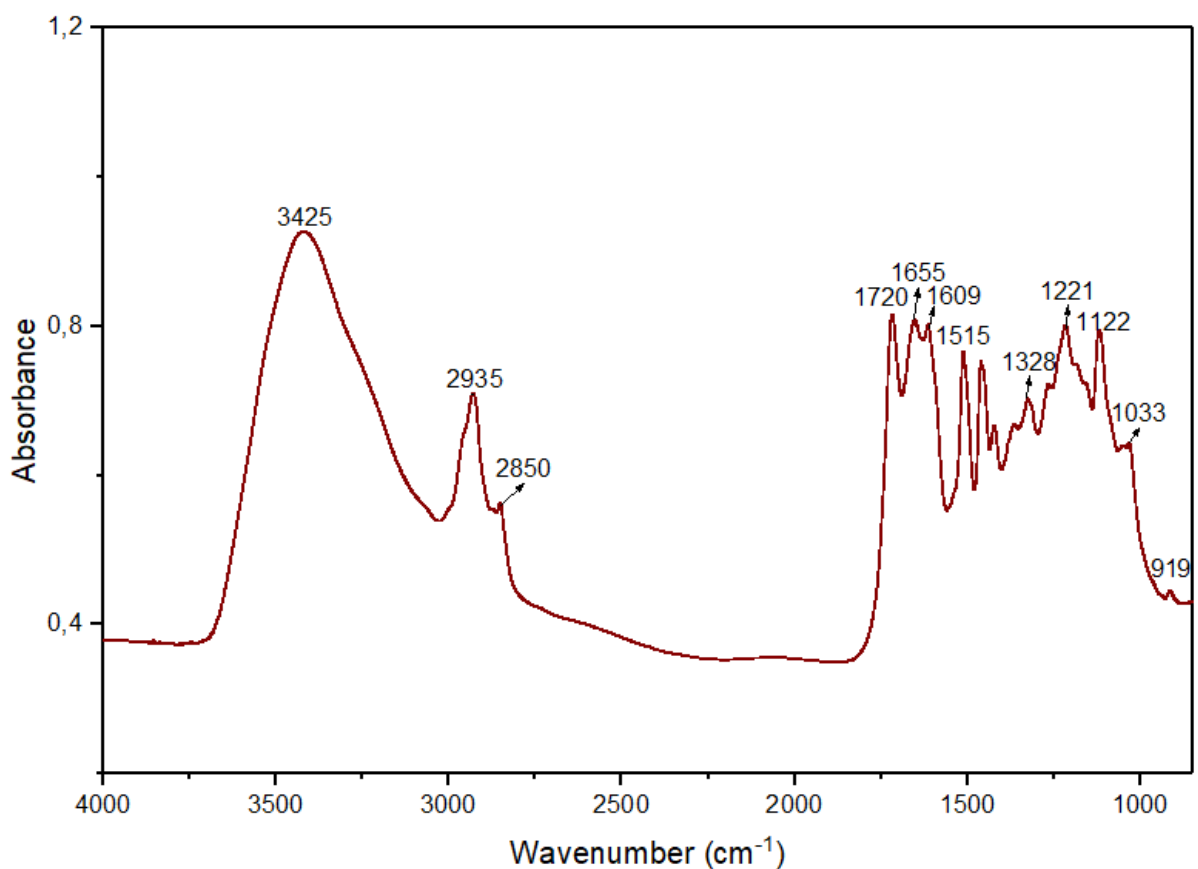
Figure 5.2: FTIR spectra for obtained rose lignin.

5.1.2   Scanning Scanning Electron Microscope (SEM)and Energy-dispersive X-ray Spectroscopy (EDX)

The characteristics of lignin, including its morphology, are dependent on sources as well as extraction conditions. Below are presented the morphological analysis by scanning electron microscopy and energy dispersive X-ray analysis.

5.1.2.1   Lignin extracted from corn stalks

Figures 5.3 and 5.4 show the lignin micrographs for ICL1 and CL-1 samples, respectively. Differences in lignin particle sizes and shape can be compared in these SEM shown images. The morphology of the sample ICL1 (Figure 5.3) shows unshaped and irregular lignin

chunks, with different sizes of particles ranging from 1 to 50 μm. In the case of CL-1 sample, shown in Figure 5.4, it is observed granulated particles with a smaller size. It is also noted some lignin clusters composed of quasi-spherical particles with diameters <1 μm. In fact, this sample was prepared by filtration using a filter paper with 1-2 μm pore size.
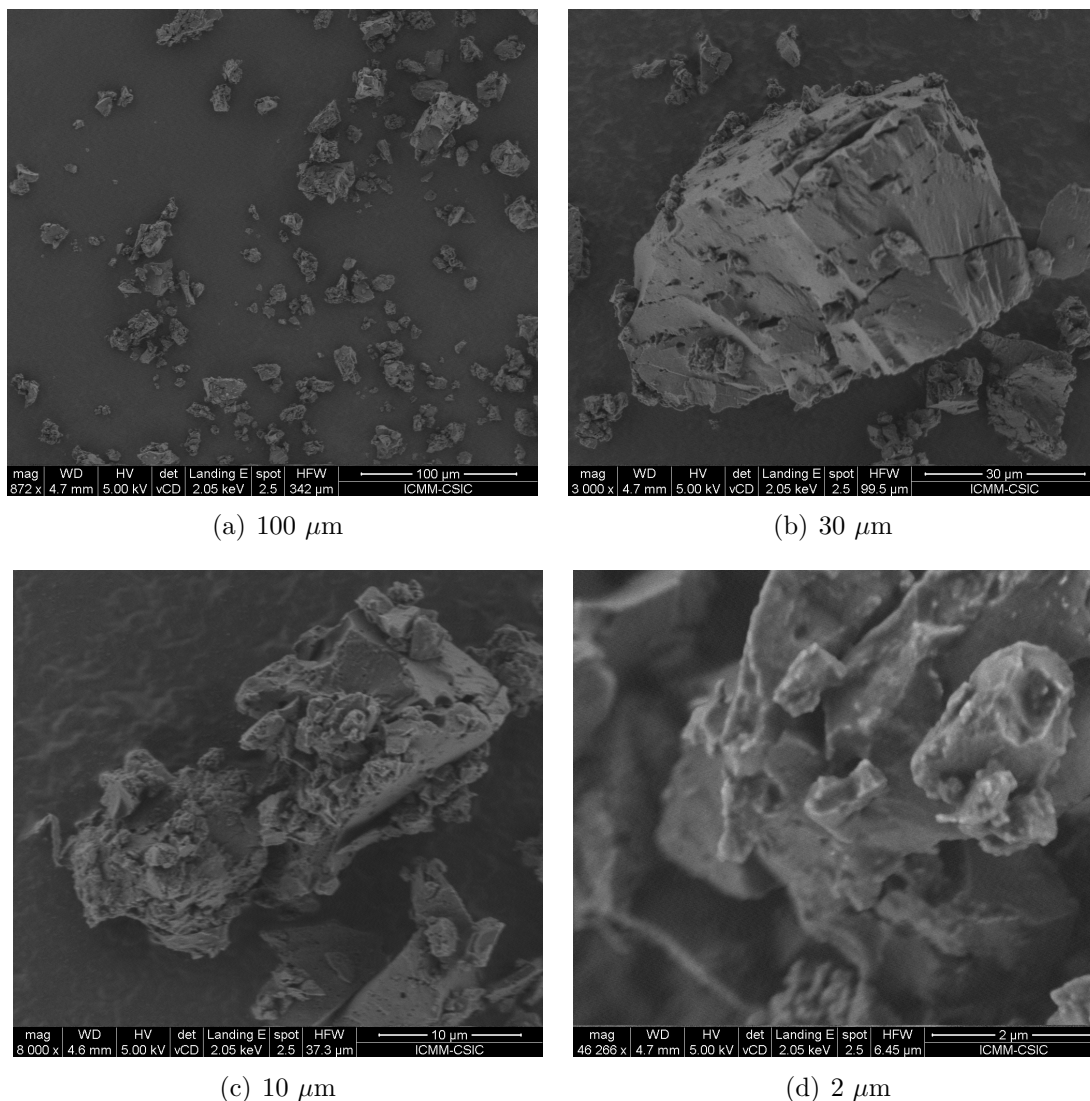

(a) 100 μm   (b) 30 μm

(c) 10 μm   (d) 2 μm

Figure 5.3: SEM images for ICL1 sample.
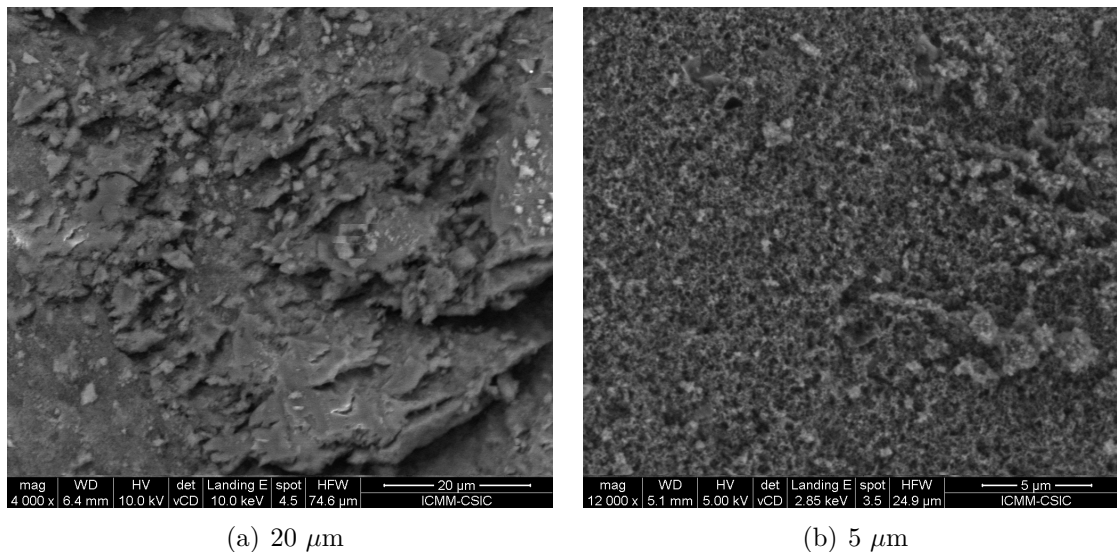
(a) 20 μm

(b) 5 μm

Figure 5.4: SEM analysis for morphology of CL-1 sample.

The elemental analysis by EDX was performed, in ICL1 sample is evident a small percentage (3.58 At%) of silicon element which can be attributed to the presence of silica maybe coming from soils, which can be taken up by plants[76]. The EDX spectra of ICL1 and CL-1 samples are depicted in Figure 5.5 and Figure 5.6, respectively, while the EDX quantitative results are represented in Table 5.2

Table 5.2: Quantitative results of ICL1 and CL-1 sample composition analyzed by EDX.

Element	ICL1		CL-1	
	Weight %	Atomic %	Weight %	Atomic %
C	69.16	74.80	67.54	73.52
O	24.90	21.62	32.33	26.42
Si	5.94	3.58	0.13	0.06
Total	100	100	100	100

As shown in the Table 5.2, the silicon content in the sample CL-1 decreases comparing to ICL1 sample, perhaps because the silicon particles were attached to large lignin particles.
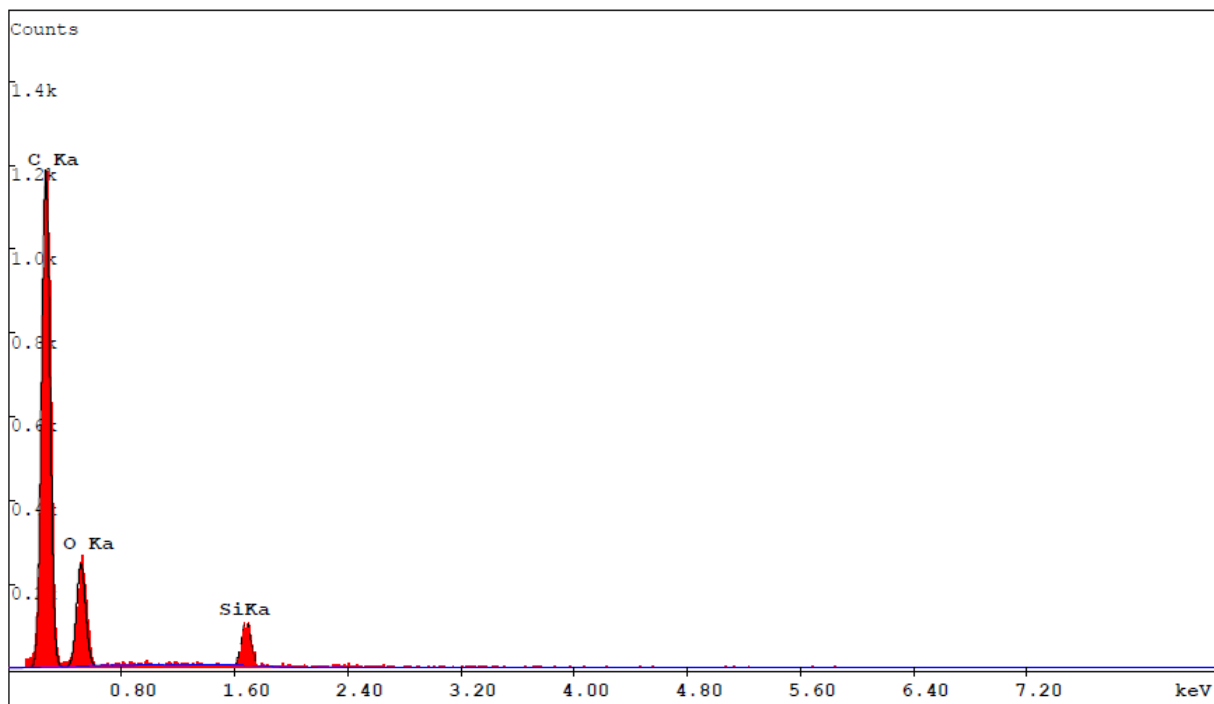
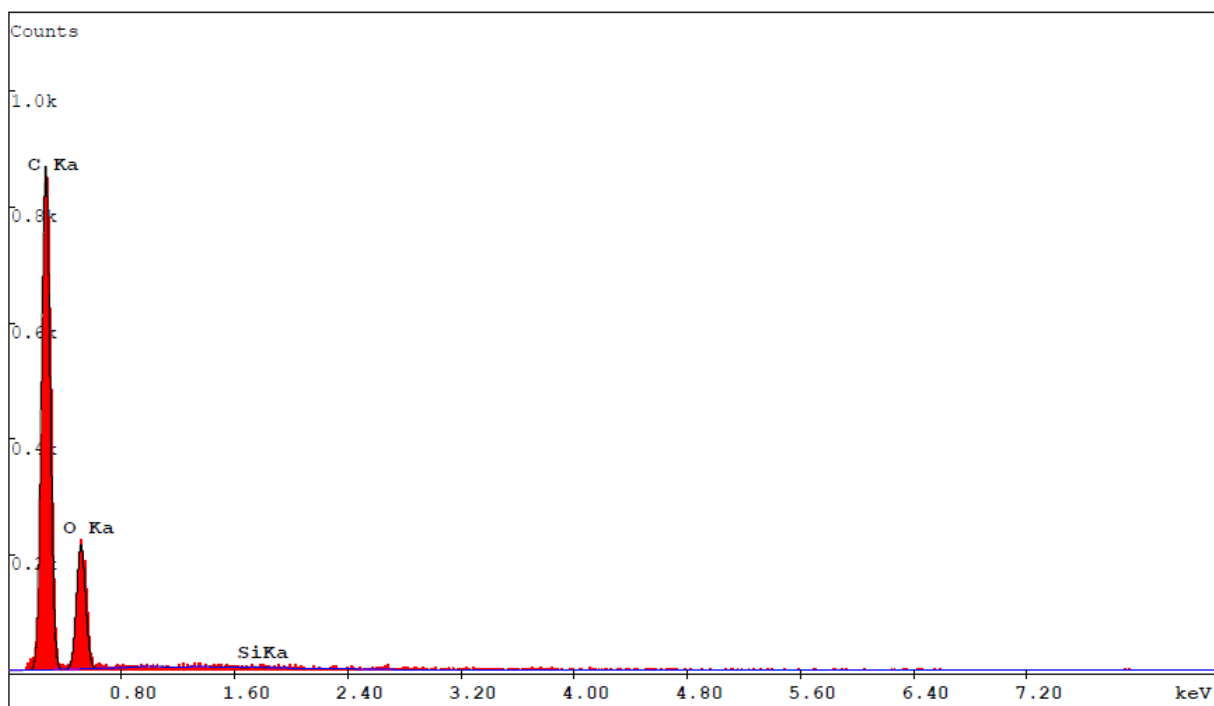*Figure 5.5: EDX spectra for ICL1 sample with a great silicon content.*

Figure 5.6: EDX spectra for CL-1 sample showing the presence of silicon content.

In the following Figure 5.7, it is shown the obtained Klason lignin after acid hydrolisis procedure. It is displayed the formation of nanoparticles of different sizes varying mainly from 80 to 200 nm. Besides, different forms are shown, most of them are spherical, showing a tendency to agglomeration.
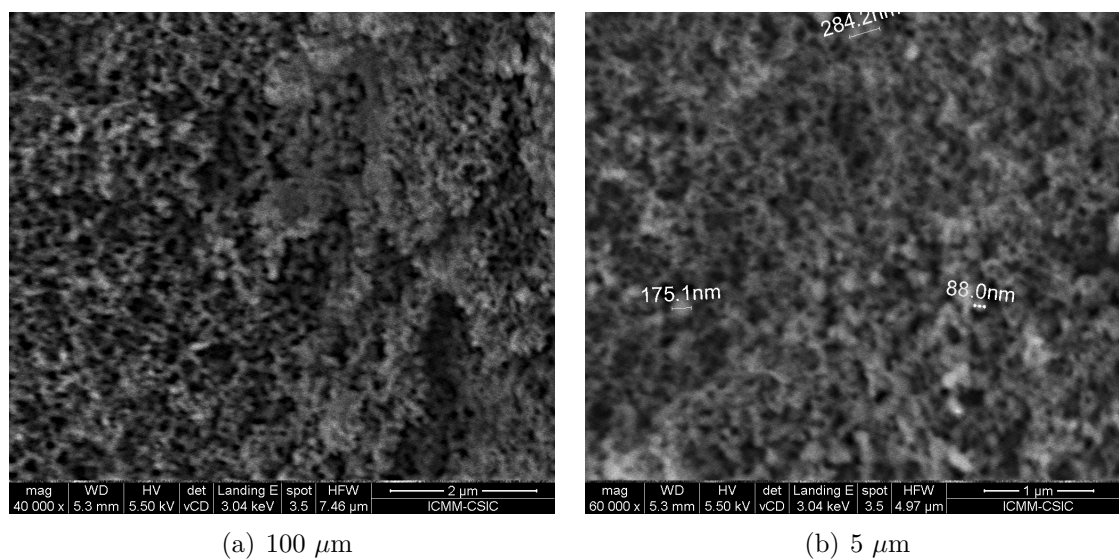

(a) 100 μm   (b) 5 μm

Figure 5.7: SEM images for corn lignin with acid treatment

By comparing this previous result with the morphology of the initial sample, a great change can be seen because at the beginning, SEM images revealed particles of micron sizes and undefined morphology.

5.1.2.2   Lignin extracted from rose stem

Morphology of IRL1 sample is exhibited in the Figure 5.8. It is important to emphasize that very little amount of insoluble rose sample was obtained. The particles observed in the background have a spherical and oval appearance with more homogenized sizes compared to the sample obtained from the corn. However, the most visible particles that can be noticed on the surface, have different shapes and sizes, although some of them show an evident spherical geometry.
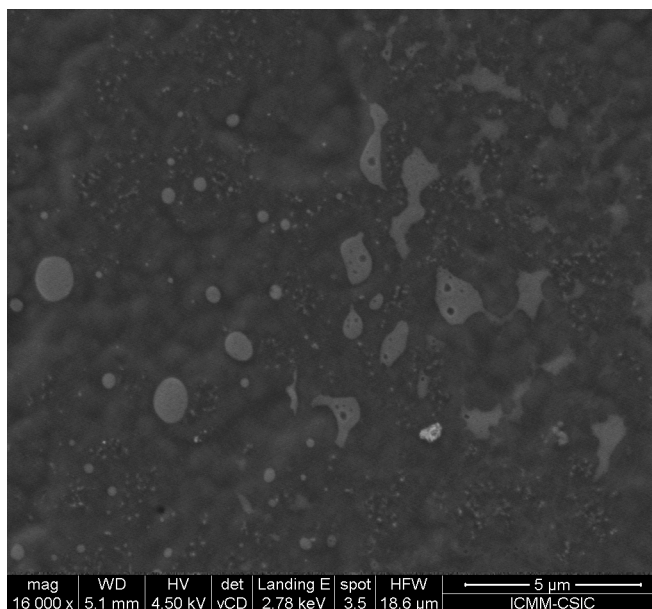
Figure 5.8: SEM analysis for IRL1 samples in which is appreciated its morphology.

After the process of filtration, morphology of lignin particles in the filtrate (RL-1 sample) was also analyzed by SEM. This result is shown in the Figure 5.9. Amorphous agglomerates consisting of nano-sized particle are observed. As depicted in the Figure 5.9(d), smaller particles with a diameter of approximately 50–100 nm are formed. Notably, the particle size obtained from the rose is smaller than that of the corn.

(a) 4 μm

(b) 1 μm

(c) 1 μm

(d) 500 nm
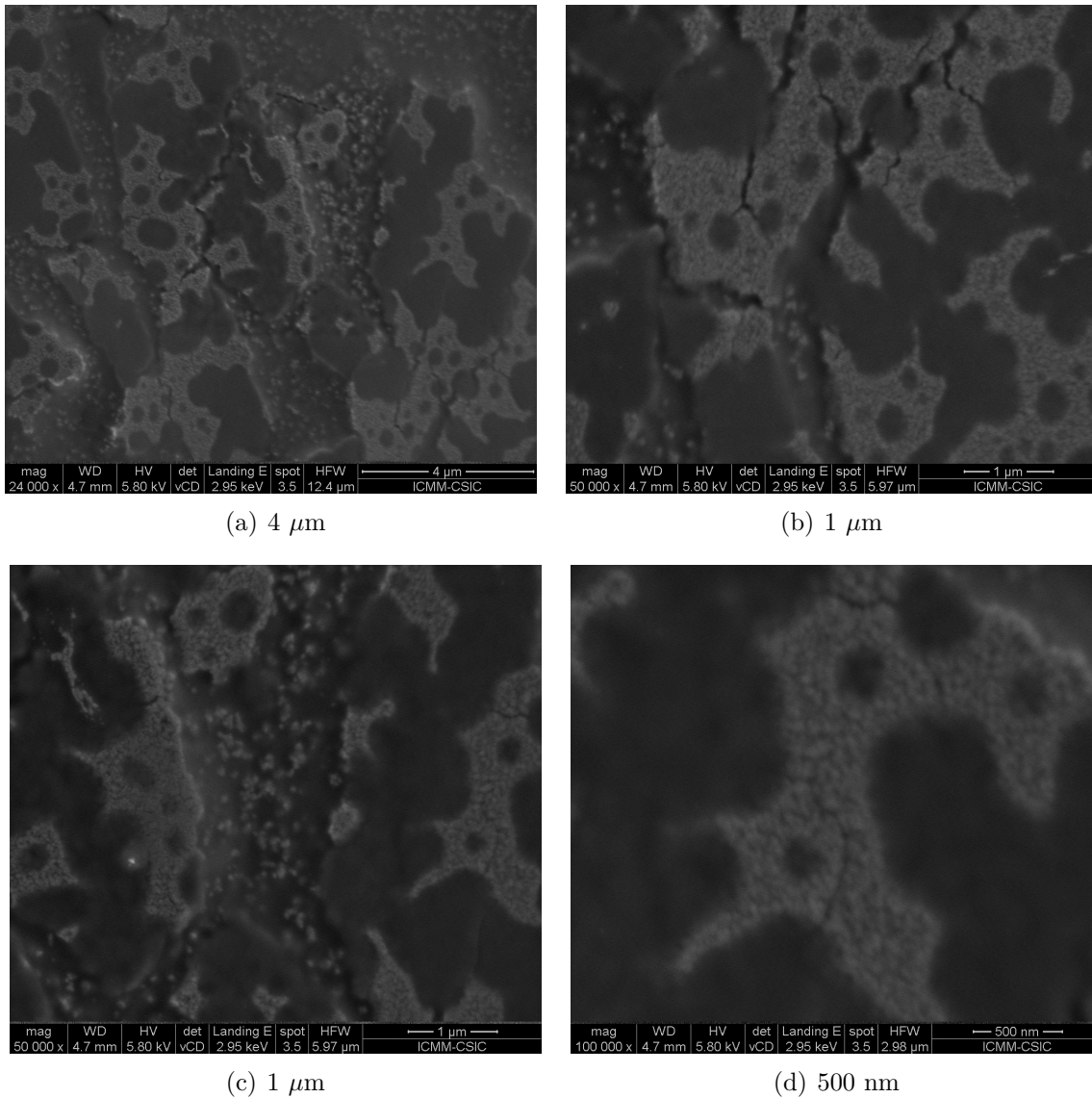
Figure 5.9: SEM analysis for morphology of RL-1 lignin sample.

In the Table 5.3 are indicated the weight and atomic percentage of the different elements found in the IRL1 and RL1 samples, while the EDX spectra of these samples are shown in Figure 5.10 and Figure 5.11.

As in the lignin IRL1 sample, consisting of larger particle size, the lignin resulting from the filtrate detected a large amount of minerals. The presence of several elements, such

as sodium (Na), iron (Fe), silicon (Si), chlorine (Cl), potassium (K), and calcium (Ca), was evidenced. For the RL-1 sample, the presence of other elements such as magnesium (Mg), and phosphorous(P) were found. In both samples, a higher proportion of carbon and oxygen is evidenced.

Table 5.3: Quantitative results of IRL1 and RL-1 sample composition analyzed by EDX.

Element	IRL1		RL-1	
	Weight %	Atomic %	Weight %	Atomic %
C	51.15	65.78	46.10	55.04
O	34.07	26.63	39.77	38.37
Na	0.41	0.23	1.06	0.71
Cl	3.61	1.52	0.86	0.38
K	3.42	1.51	5.20	2.02
Ca	0.71	0.26	2.40	0.92
Si	0.81	0.38	—	—
Fe	5.82	3.69	—	—
P	—	—	2.66	1.32
Mg	—	—	1.95	1.24
Total	100	100	100	100

The number of inorganic elements present in the lignin of the rose is much higher than that present in the corn, which can be explained by the origin of the agriculture residues. In this study, the weight percentage of ash in the IRL1 sample covers approximately 7% of the quantitative composition of rose lignin while the RL-1 sample exhibited a mineral content above 6% as reported in Table 5.3. Literature reports that inorganic minerals like Al, Si, S, Ca, Cl, P, Mg, K, Ca and Ti, are very common in the ashes of lignin from agricultural waste,[77,78] ranging from 2% to 4% of ash content[79]. Also, the presence of high mineral content in floral stalks may be due to the importance of nutrient transport.[80].
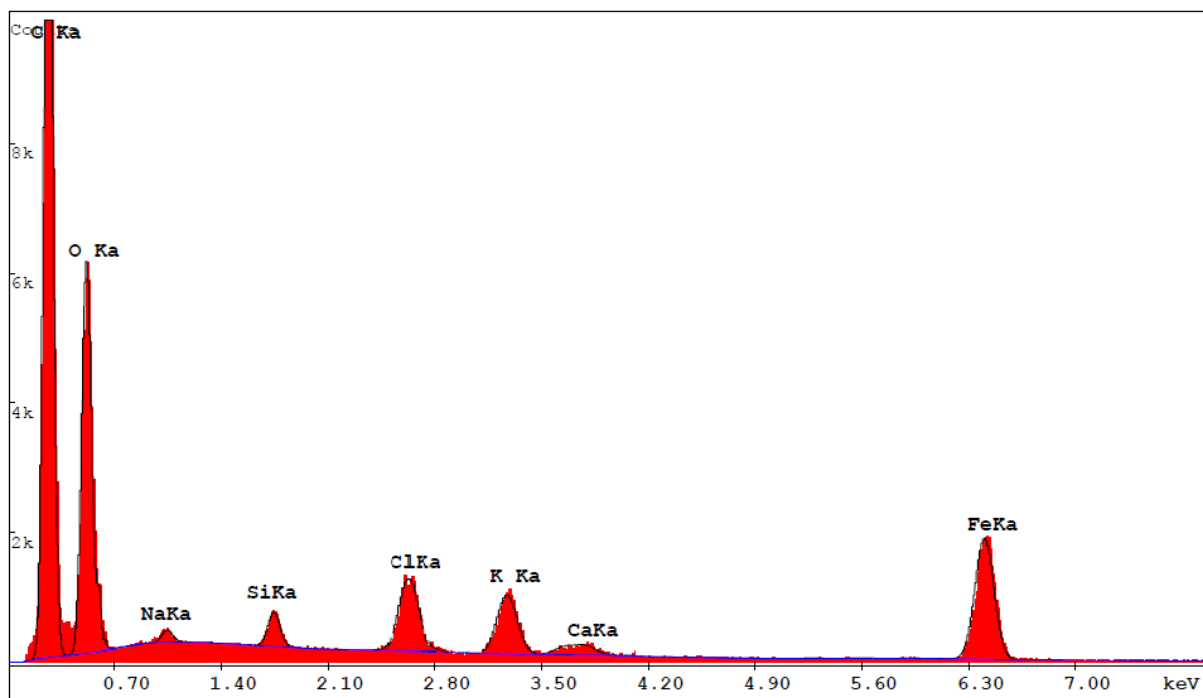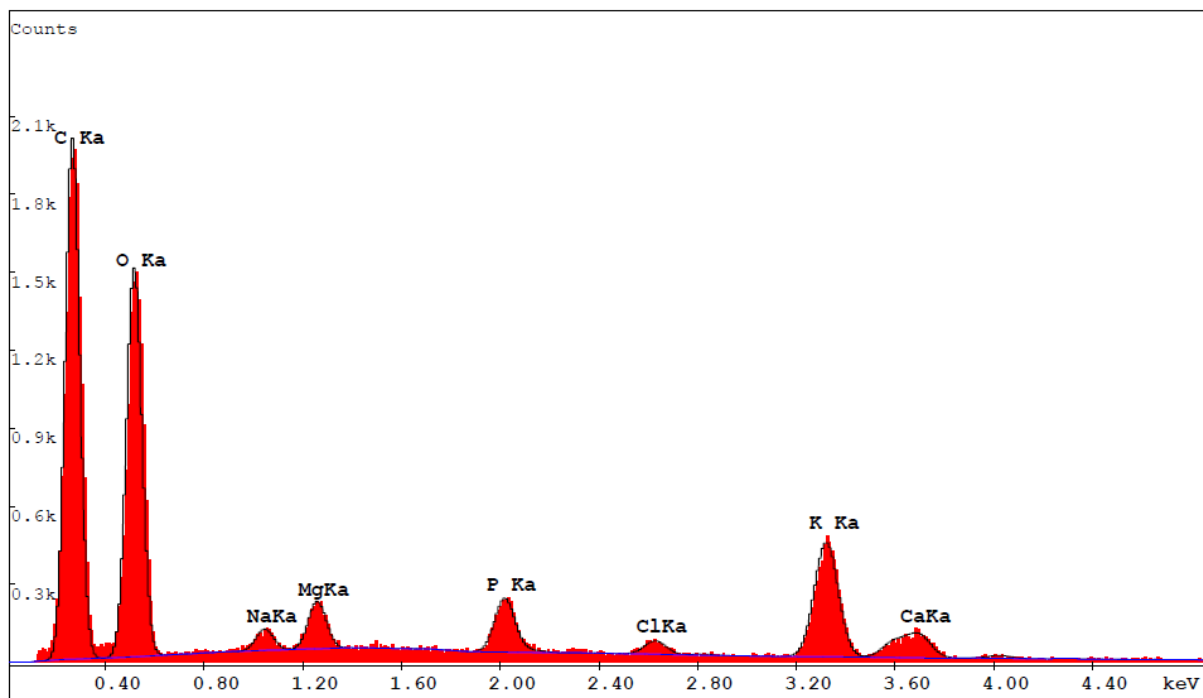
Figure 5.10: EDX spectra for IRL1 sample.

Figure 5.11: EDX spectra for RL-1 sample.

Because the initial purpose of this project was to obtain pure lignin, at least with a low percentage of impurities, the acid hydrolysis treatment was performed in the RL-1 sample, in order to remove the inorganic impurities mentioned. As in the case of corn, after the acid hydrolysis treatment rose lignin also showed significant changes, as is shown in Figure 5.12. In that case, spherical particles with an homogeneous size distribution, around 60 nm, are observed.

(a) 1 μm   (b) 1 μm
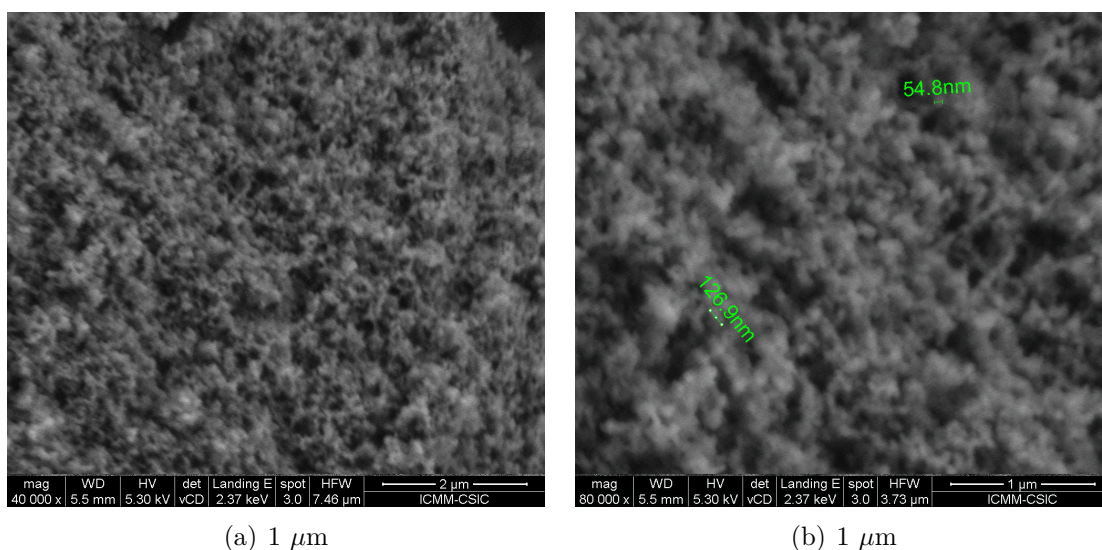
Figure 5.12: SEM morphology analysis of the rose lignin sample with acid treatment.

5.1.3 Dynamic Light Scattering (DLS) and Zeta Potential

Particle size distributions and Zeta potential values of lignin samples were analyzed. With respect to Dynamic Light-Scattering measurements, they were performed for CL-1 and RL-1 samples to evaluate the influence on particle size, distributions and polidispersity, due to pH changes in the lignin extracted from rose and corn. In Zeta potential analysis, measurements at different pH values allowed to provide information on the functional groups present on the surface, i.e. the presence of acidic or basic functional groups.[81] Two

measurements were carried out for each sample, and from these the mean was calculated. These mean results are summarized in Table 5.4 and in Figure 5.17.

5.1.3.1   Lignin extracted from rose

According to the DLS results for the RL-1 sample, which are summarized in Table 5.4, it can be mentioned that a tendency to decrease the particle size was observed as the pH dispersion increased. At the lower pH tested (pH 3.2), particles exhibited the highest mean diameter (753.53 nm), with a particle size distribution in a range from 300 nm to 600 nm and 900-2300 nm, depicted in Figure 5.13, in which is represented the number based particle size distribution in a semi-logarithmic plot. The PDI of this sample showed a value of 0.302. The polydispersity value corresponds to disperse systems with uniform distribution[82]. The Zeta potential at pH 3.2 is the lowest absolute value (-2.64 mV) among all pH conditions evaluated, suggesting the particle aggregation. Indeed, this is consistent with the DLS result, which showed that the lower the pH is the larger the mean diameter is, as a consequence of particles aggregation.

Table 5.4: Mean diameter of lignin samples at different pH values, with corresponding polydispersity index from DLS analysis, and Zeta potential

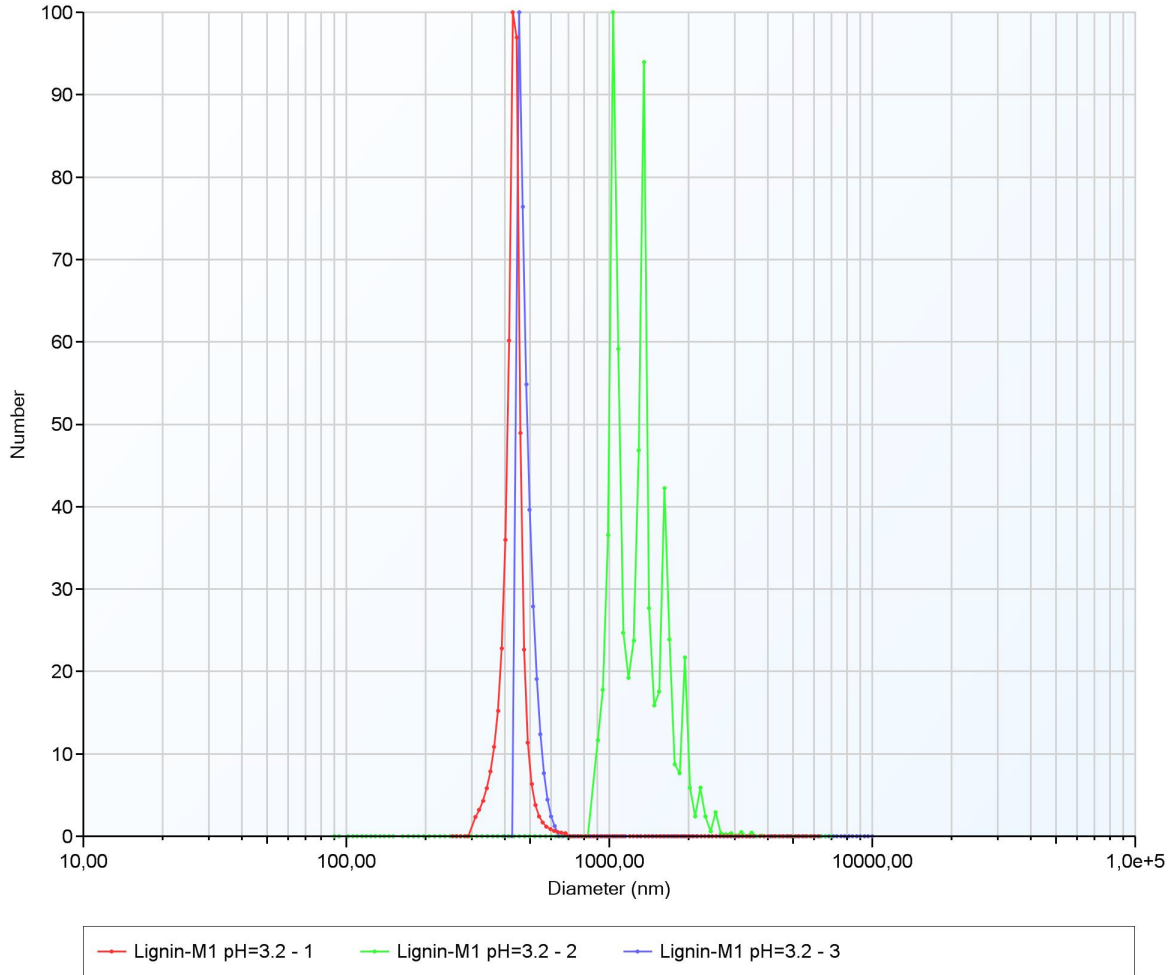| pH	Mean Diameter, $D_m(nm)$	Polydispersity, PDI	Mean Zeta Potential (mV)
3.2	753.53	0.302	-2.64
5	259.38	0.299	-28.07
7	118.91	0.264	-20.41
9	189.77	0.294	-33.17

Figure 5.13: Results from number concentration distributions of sample of lignin from rose with pH 3.2

As seen in the Table 5.4, all measurements of the Zeta potentials of lignin particles were negative. The fact that negative values were obtained can be attributed to the negative charge of phenols, and possible adsorption of hydroxyl ions (OH^-)[83,84], which is expected for hydrophobic surfaces in contact with water. The hydroxyl ions contribute to increasing the negative values of the Zeta potential, causing greater electrostatic repulsion. The high negative Zeta potential values obtained for most of the samples suggest an adequate electrical double layer repulsion between suspended particles, preventing their aggregation[83].

At pH 5, the mean diameter decreased significantly to a value of 259.38 nm. Moreover, in the semi-logarithmic plot of number based particle size distribution, shown in the Figure 5.14, a more uniform particle distribution was obtained in a range diameter from 200 to 400 nm. This distributions observed have a lower polydispersity index (PDI) than that obtained for the dispersion with pH 3.2 .
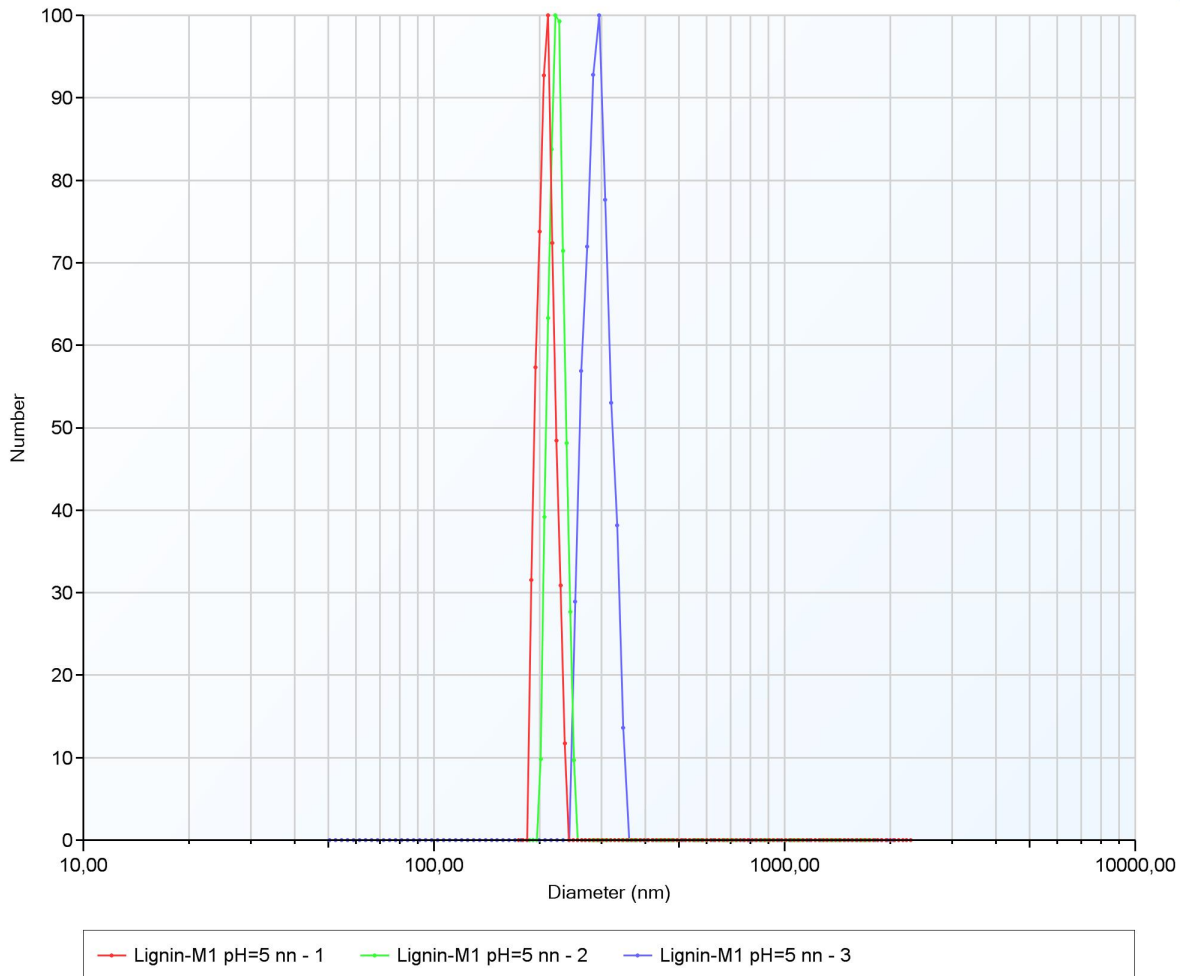

Figure 5.14: Results from number concentration distributions of sample of lignin from rose with pH 5.

Although in general the results showed a increase in Zeta potential with the increase in pH from 3 to 9, it can be seen that electrokinetic potential did not present a monotonic increase, but it presented a decrease at pH 7. The changes in particles size with the pH

of dispersions can be due to an interplay between two processes; one of them associated with the dissolution of the particles, implying a size decrease, while the other one corresponds to a Ostwald ripening process, which leads to larger particle diameters[85]. This can be noted in the Figure 5.15, in which is shown that for sample with pH 7, a multimodal number based particle size distribution was exhibited. Three ranges of particle diameter are shown in this Figure 5.15 corresponding to formation of both smaller and larger particles with respect to the pHs analyzed, suggesting the competition between the both previously mentioned processes. This can explain the fact that the size distribution for run number 3 (green line in the figure) differed greatly from those of the first run (red line in the figure) and the second run (blue line in the figure), these last two being very similar. The mean value of size distribution for the third run corresponded to a diameter smaller than 50 nm (particle dissolution predominates), while for run number 1 and run number 2 distributions, the mean diameters correspond to values <150 nm and <400 nm, respectively (Ostwald ripening predominates).

The Zeta Potential for the dispersion with pH 7 was found to be -20.41 mV, which corresponds to a value ten times greater than that obtained for the lowest tested pH (3.2), but smaller than that obtained for the dispersion with pH 5. This behavior can also be explained with the occurrence of the two particle size modulating processes. The PDI for this dispersion resulted in 0.264, corresponding to a homogeneous dispersion despite presenting a multimodal size distribution, taking into account that the smaller the PDI value is the more homogeneous particles dispersion is.
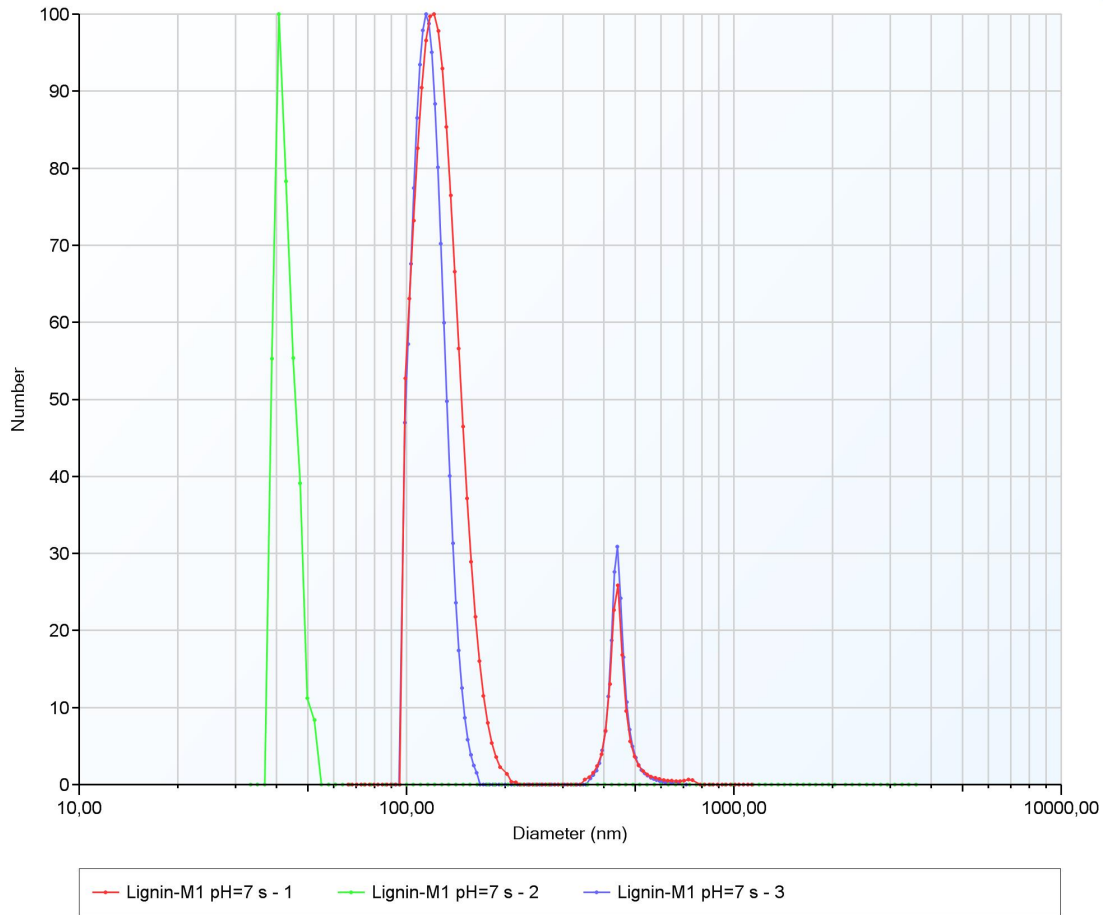
Figure 5.15: Results from number concentration distributions of sample of lignin from rose with pH 7.

Finally, sample with pH 9 presented a particle size of 189.77 nm and a Zeta potential of -33.17 mV. These values are consistent with the fact that the more negative values of Zeta potential are, the greater the stability in the particles is. So, this high negative value for Zeta potential prevents agglomeration and leads to a smaller particles. The number based particle size distribution exhibits two ranges of particle size distribution by number: 100-300 nm and 600-900 nm as can be seen in the Figure 5.16, also exhibits a low polydispersity index of 0.294.
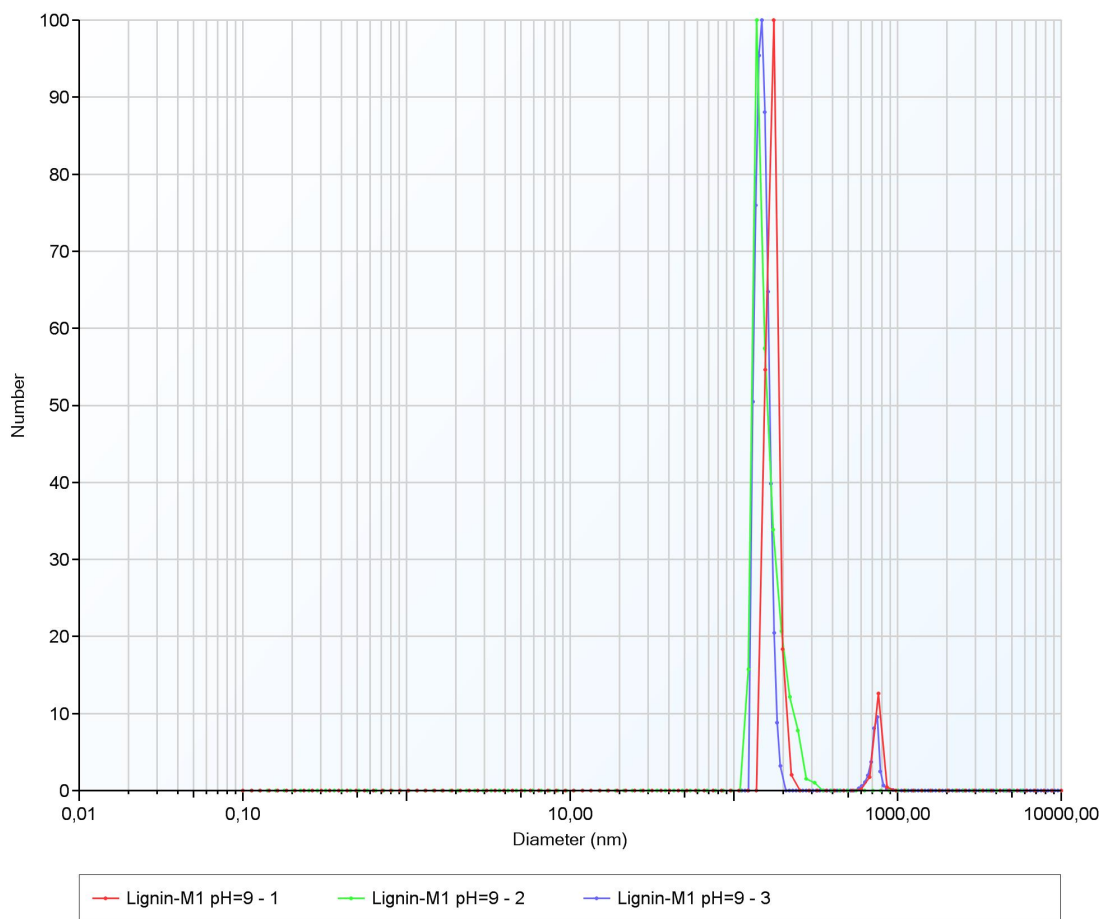
Figure 5.16: Results from number concentration distributions of sample of lignin from rose with pH 9.

From the results obtained it can be mentioned that the lignin particles present a greater stability in dispersions with pH ranging from 5 to 9, preventing the particles aggregation. This is in agreement with literature that reports stability of nanoparticles formed from softwood Kraft lignin at pH 4–10.[84] In Figure 5.17 Zeta Potential values are shown for each measurement performed at all dispersions analyzed with different pH. In such figure, a tendency to high negative values of Zeta Potential can be seen when the pH increases.
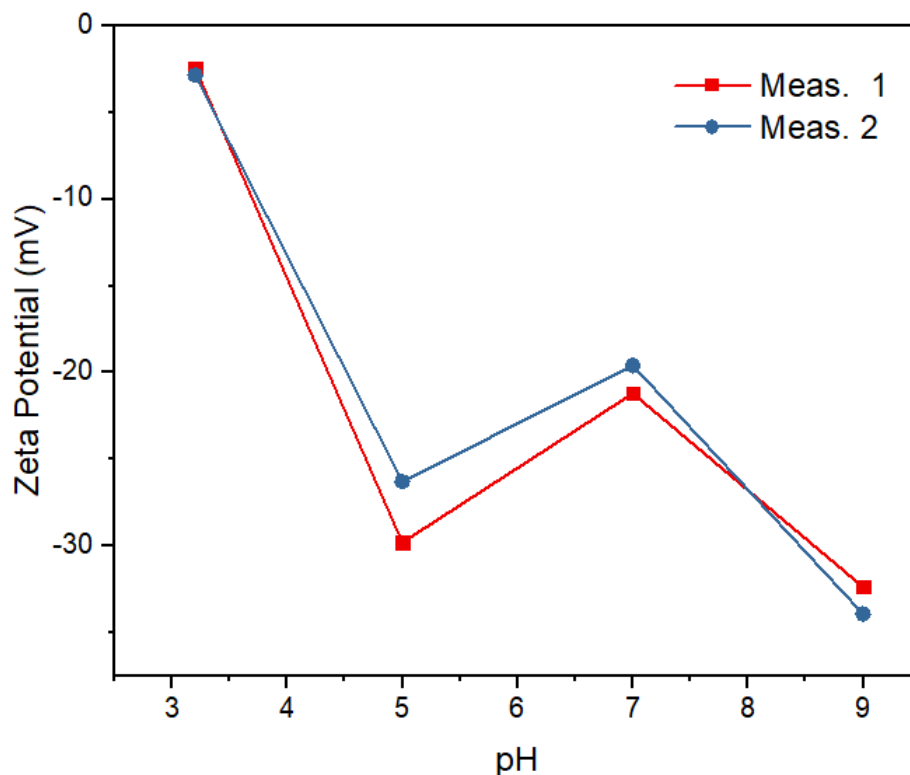
Figure 5.17: Zeta Potential measurements of RL-1 sample.

5.1.3.2   Lignin extracted from corn

The procedure carried out for lignin extracted from corn was the same as that described in previous section for lignin from rose. Unfortunately, particles of lignin from corn were too large that DLS and Zeta Potential analysis could not be executed. This is in accordance with Scanning Electron Microscopy (SEM) images, which revealed large particles of lignin from corn.

5.1.4   UV-VIS Spectroscopy

Lignin absorbs ultraviolet light in characteristic regions based on its aromatic nature and chromophoric groups. This fact has been reported in the literature[86], as well as it was proved in this project by the obtained UV-Visible absorption spectra, shown in the

Figures 5.18 and 5.19. In the case of rose lignin, UV-Vis spectrum, given in the Figure 5.18 shows two absorption peaks around 240 and 270 nm, and a soft shoulder around 350 nm. These two first bands are assigned to the presence of free and etherified hydroxyl groups, while the signal at around 350 nm is attributed to $\pi \rightarrow \pi^*$ transition corresponding to non-conjugated phenolic groups as sinapyl alcohol (S), coniferyl alcohol (G) and p-coumaryl alcohol (H), and the transition $n \rightarrow \pi^*$ from conjugated phenolic groups in lignin such as p-coumaric or ferulic acid. However, the signal appearing at 350 nm is slightly shifted with respect to that is reported in the literature (320 nm), perhaps due to the different chemical environmental associated to lignin structures, and by a slight bathochromic effect (red shift) due to solvent effect.[87]
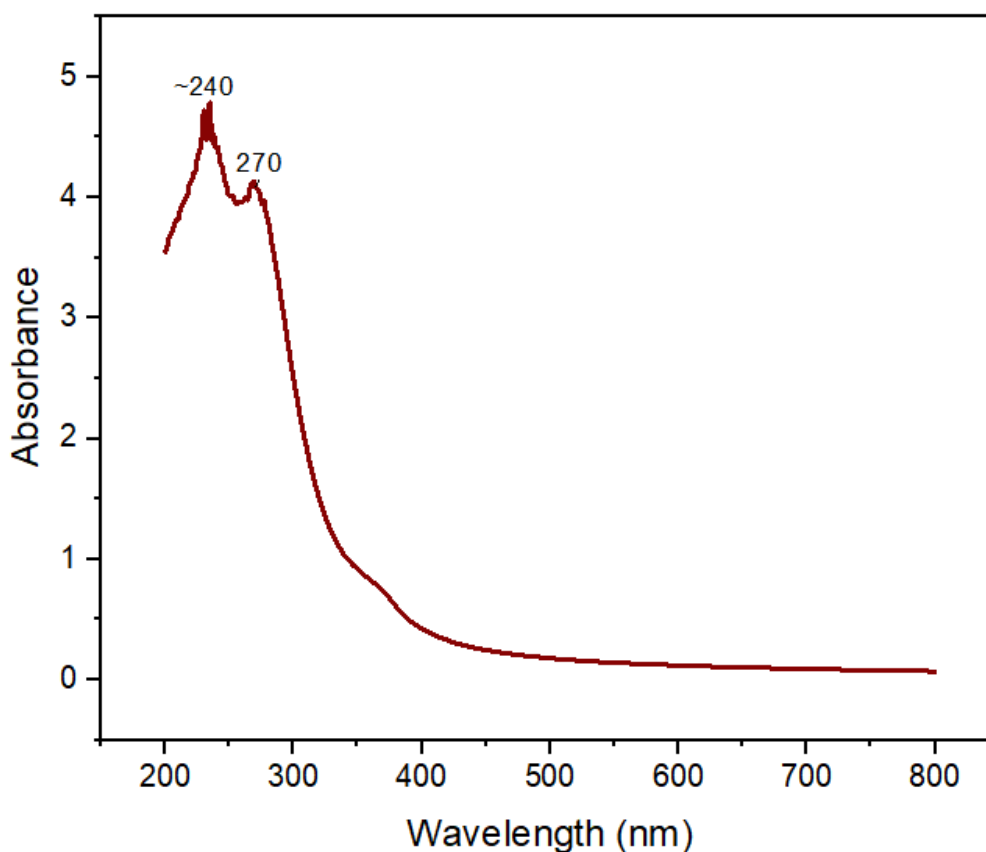
Figure 5.18: UV-Vis absorption spectra of RL-1 sample.

With respect to lignin extracted from corn, in the UV-Vis spectrum shown in the Figure 5.19, although with lower resolution, the bands corresponding to same previously mentioned transitions can be appreciated. A shift of the bands by the chemical environmental and solvent effect is observed again.
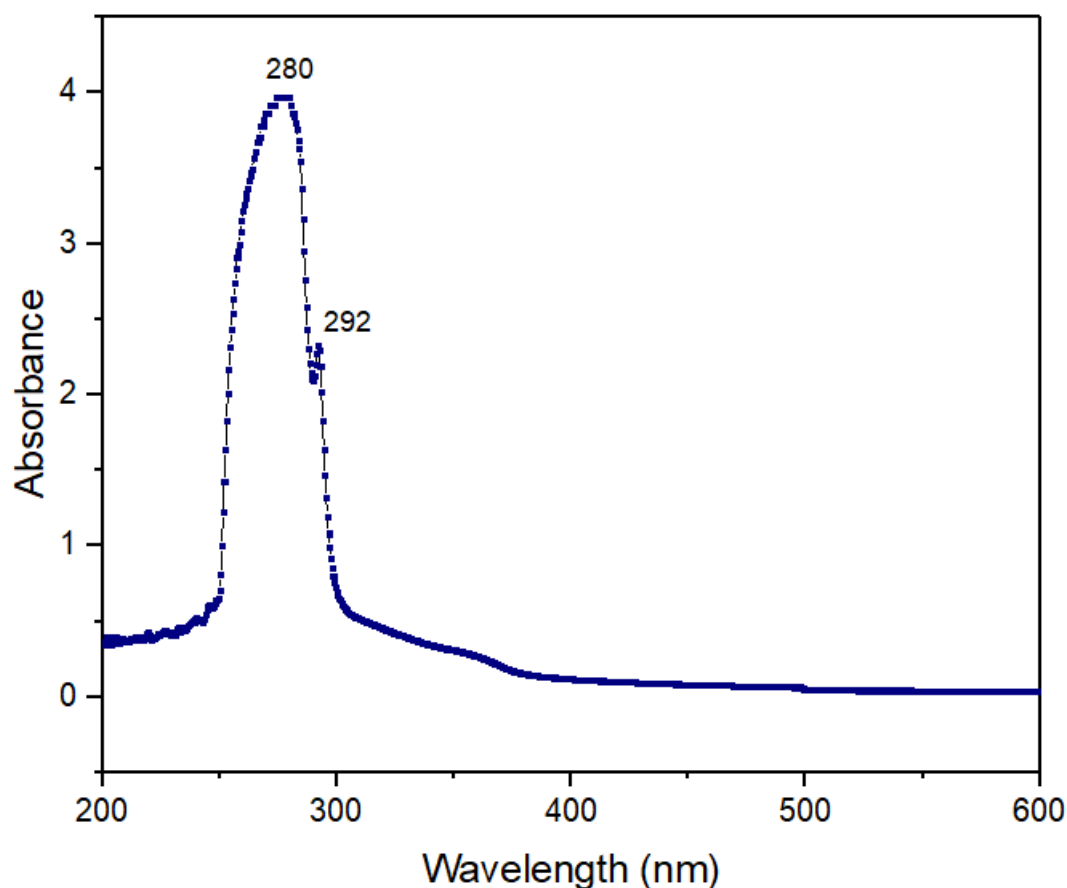
Figure 5.19: UV-Vis absorption spectra of CL-1 sample.

5.1.5   X-ray Diffraction

Figure 5.20 shown the XRD diffraction pattern of RL-1 and CL-1 samples. In both spectra is exhibited a broad halo peak over the range 8°-32°/2θ, with the average peak at 2θ=21.680°. The absence of crystalline peaks was expected as shown in the CL-1 sample because lignin is a natural amorphous polymer. Similar XRD patterns has already

been reported in previous works, for example, lignin extracted from sugarcane bagasse through aqueous hydrotropic solutions reported the diffraction angle $22.37°/2\theta$,[88] while for hardwood acetic acid lignin is reported at about $22°/2\theta$.[89] However, in the XRD pattern from rose source, a small peak is appreciated at around $15°/2\theta$ which can be attributed to the presence of compounds as a result of the high content of inorganic compounds in the RL-1 sample, as previously detailed in the EDX results (Table 5.3). These differences in the patterns are due to the different types of lignin.

In the Figure 5.20, is also shown the XRD pattern for Kraft lignin (green line in the figure), which was provided by a paper company. A good comparison of Kraft lignin can be appreciated with the lignin extracted from corn and rose in this project.
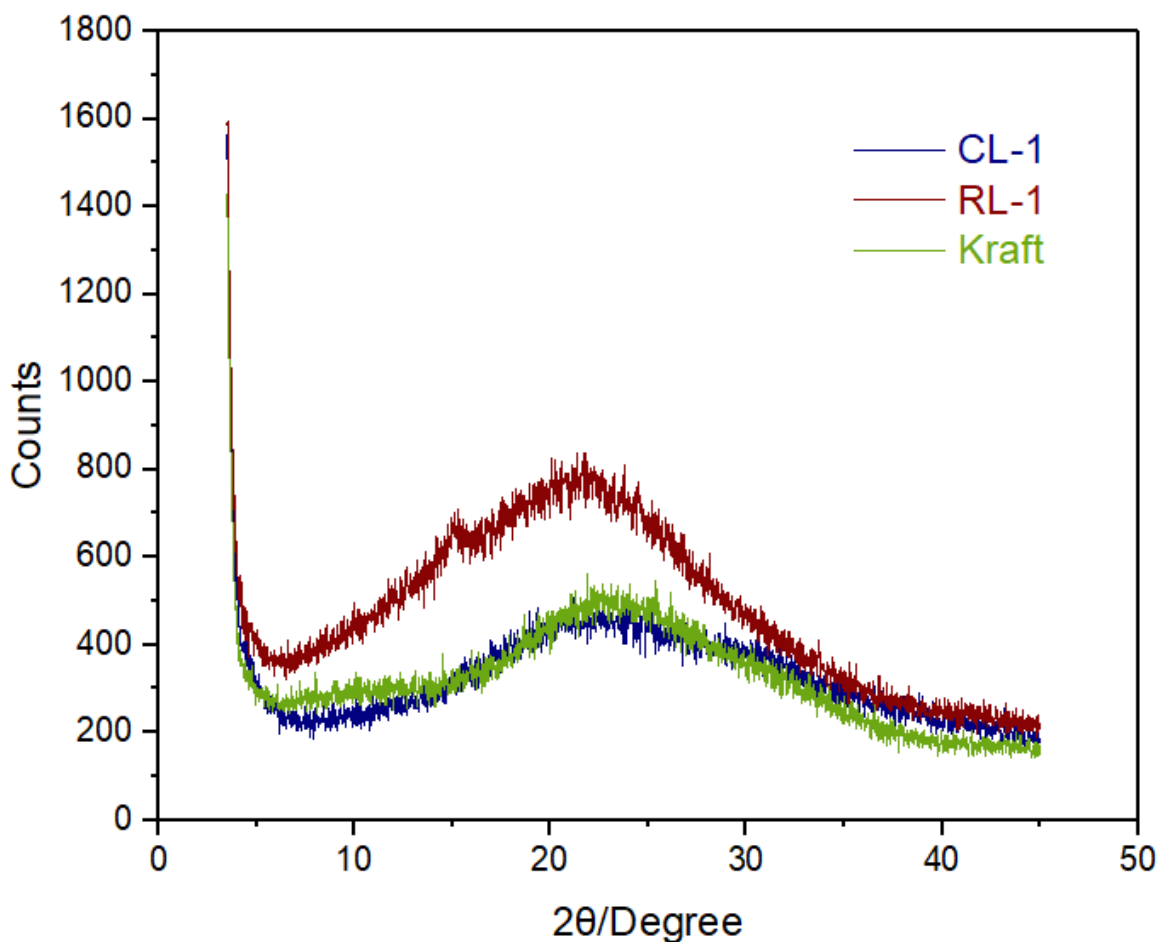

Figure 5.20: X-ray diffraction analysis of RL-1, CL-1 and Kraft lignin samples.

5.2   Evaluation of UV-absorption capacity of lignin

The measurements were made using PVA films blended with different lignin concentration, being the wavelength range detected by the digital light meter between 280-400 nm, which includes UVA and UVB regions. The results are shown in the Table 5.5. Films with higher concentrations of lignin showed higher levels of UV absorbance from sunlight. Effective results are obtained with PVA films with additions of 2% and 4% lignin content showing an absorbance greater than 90%. In spite of the fact that the absorbance percentage of the films prepared through bonding of PVA with low lignin content were lower than those previously evaluated, the results are very good. Control sample film with only PVA did not present absorbance remarkable, with UV absorbance values less than 10%.

Table 5.5: Absorbance percentage results of PVA based films with different concentrations of lignin

Films preparation	% of Absorbance
PVA	1.61
PVA + 0.5% lignin	61.97
PVA + 1% lignin	72.39
PVA + 2% lignin	98.05
PVA + 4% lignin	99.74

Films with 2% and 4% lignin content and the control sample film, were subject to a second test to study the UV properties stability. Films were irradiated under the influence of a homemade chamber operated by a UV lamp (185nm bulb) over more than 3 hours in order to simulate the material degradation by means of UVC energy. Then, the percentage of absorbance was measured as in the previous step, through direct exposure to sunlight. Table 5.6 details the results. The films with contents of 2% and 4%

lignin, showed a stability of their UV absorption properties, i.e. were not affected by the radiation assay with the UVC lamp. PVA film shows a slightly increase of UV absorption from 1.61% to 13.39% which can be explained by the possible appearance of new chromophores. Research reports that PVA under UV influence undergoes to reactions of main chain scission, oxidation and loss or conversion of side groups.[90] In addition, the content of carbonyl groups increases because the UV treatment is executed in oxygen-containing atmosphere.

Table 5.6: Absorbance percentage results of control film and PVA based films with lignin contents of 2% and 4% after stability test.

Films preparation	% of Absorbance
PVA	13.39
PVA + 2%lignin	99.09
PVA + 4%lignin	99.51

5.2.1 Comparison with commercial solar protectors

In order to analyze the skin care for UV rays, different commercial sunscreens were analyzed and compared with a moisturizing commercial cream alone and with lignin added to it. Table 5.7 provides the results from this assay.

Table 5.7: Absorption percentage of sunscreens and cream with lignin addition.

Films preparation	% of Absorbance
Umbrella 100 SPF	97.08
Bioderma 50 SPF	93.79
Nivea cream	48
Nivea cream + lignin	85.46

Commercial sunscreen with a SPF of 100, shows the best result with a greater percentage of absorbance of sunlight. Also, a good value is obtained from the second commercial sample corresponding to Bioderma 50 SPF. It is evident that in the soft moisturizer that lacks sun protection, the absorbance of the sun's rays has a low value. However, when adding the low lignin content, the UV absorbance increases from 48% to 85.46%. This value obtained is very good and can increase as the concentration of lignin increases. This result is in agreement with previous studies demonstrate that the addition of lignin to commercial sunscreens provide an enhancement of solar protection effect.[91]

CHAPTER 6

CONCLUSION AND RECOMMENDATION

6.1 Conclusions

- The extraction of lignin from different sources (rose stem and corn stalk) using organic solvents showed promising results. Also, extraction from rose stems resulted in a more homogeneous size micrometric distribution of particles compared with the extraction from corn stalks.

- The characterization of lignin through FTIR displayed that lignin spectra obtained from both sources, corn and rose, showed characteristic lignin bands. However, the presence of mineral impurities was known through EDX, which were removed through an acid hydrolysis treatment. This procedure also allowed to obtain particles of nanometric size. Besides, DLS data reveals that size of lignin particles exhibit a dependence with the pH of dispersion.

- UV absorption properties of lignin were tested by preparing PVA films with small additions of lignin, and through the addition of lignin to a moisturizing commercial cream. The films showed excellent UV absorption with the increase in lignin volume concentration, greater absorption was evidenced. In addition, when lignin

particles were added to the moisturizing commercial cream, the improvement of UV absorption was evident. This project confirmed the inherent property of lignin as a UV blocker.

6.2 Recommendation

- To execute an analysis of the mechanical properties of PVA-based films to observe the effect of lignin additions.

- To carry out toxicological analysis of the lignin particles obtained.

BIBLIOGRAPHY

[1] M. Nuruddin, A. Chowdhury, S. Haque, M. Rahman, S. Farhad, M. Jahan and M. Quaiyyum, *Cellulose Chemistry and Technology*, 2011, **45**, 347–354.

[2] R. A. N. Wolfgang G. Glasser and T. P. S. (Eds.), *Lignin: Historical, Biological, and Materials Perspectives*, American Chemical Society, 2000.

[3] S. Fatma, A. Hameed, M. Noman, I. Sohail, M. Shahid, M. Tariq and R. Tabassum, *Protein Peptide Letters*, 2018, **25**,.

[4] M. Bernal, S. Sommer, D. Chadwick, C. Qing, L. Guoxue and F. Michel, in *Current Approaches and Future Trends in Compost Quality Criteria for Agronomic, Environmental, and Human Health Benefits*, 2017.

[5] B. Hinterstoisser and L. Salmén, *Vibrational Spectroscopy - VIB SPECTROSC*, 2000, **22**, 111–118.

[6] M. Asif, in *Sustainability of timber, wood and bamboo in construction*, 2007.

[7] P. Bajpai, *Pretreatment of Lignocellulosic Biomass for Biofuel Production-Structure of Lignocellulosic Biomass*, 2016.

[8] F. Xu, in *Structure, Ultrastructure, and Chemical Composition*, 2010, pp. 9–47.

[9] A. Pandey, T. Bhaskar, M. Stocker and R. Sukumaran, *Recent Advances in Thermo-Chemical Conversion of Biomass*, 2015.

[10] L. Gottumukkala, A. Mathew, A. Abraham and R. Sukumaran, in *Biobutanol Production: Microbes, Feedstock, and Strategies*, 2019, pp. 355–377.

[11] A. Sebayang, H. Ong, H. Masjuki, S. Dharma, a. bahar and T. M. I. Mahlia, *RSC Adv.*, 2016, **6**,.

[12] V. Pasangulapati, K. Ramachandriya, K. Ajay, M. Wilkins, C. Jones and R. Huhnke, *Bioresource Technology*, 2012, **114**, 663–9.

[13] M. Witzler, A. Alzagameem, M. Bergs, B. El Khaldi-Hansen, S. Klein, D. Hielscher, B. Kamm, J. Kreyenschmidt, E. Tobiasch and M. Schulze, *Molecules*, 2018, **23**, 1885.

[14] J. Acosta, P. I. Torres Chavez, B. Ramirez-Wong, C. Lopez Saiz and B. Montano Leyva, *Bioresources*, 2016, **11**,.

[15] Q. Liu, L. Luo and L. Zheng, *International Journal of Molecular Sciences*, 2018, **19**, 335.

[16] M. Brebu and C. Vasile, *Cellulose Chemistry and Technology*, 2010, **44**, 353–363.

[17] E. Ehrnrooth, *Journal of Wood Chemistry and Technology - J WOOD CHEM TECHNOL*, 1984, **4**, 91–109.

[18] A. Alzagameem, S. Klein, M. Bergs, T. Do, I. Korte, S. Dohlen, C. Hüwe, J. Kreyenschmidt, B. Kamm, M. Larkins and M. Schulze, *Polymers*, 2019, **11**, 670.

[19] Z. Mahmood, M. Yameen, M. Jahangeer, M. Riaz, A. Ghaffar and I. Javid, in *Lignin as Natural Antioxidant Capacity*, 2018.

[20] C. Pouteau, P. Dole, B. Cathala, L. Avérous and N. Boquillon, *Polymer Degradation and Stability*, 2003, **81**, 9–18.

[21] N. Li, Y. Chen, H. Yu, F. Xiong, W. Yu, M. Bao, Z. Wu, C. Huang, F. Rao, J. Li and Y. Bao, *RSC Adv.*, 2017, **7**, 20760–20765.

[22] M. Paulsson and J. Parkås, *Bioresources*, 2012, **7**, 5995.

[23] V. Dumitriu, S.; Popa, *Polymeric Biomaterials: Structure and Function*, CRC Press, Boca Raton, USA, 2013, vol. 1.

[24] S. Mansfield, *Current opinion in biotechnology*, 2009, **20**, 286–94.

[25] N. Vu, H. Tran, B. Nhi, C. Vu and H. Nguyen, *International Journal of Polymer Science*, 2017, **2017**, 1–8.

[26] P. Wild, W. Huijgen and R. Gosselink, *Biofuels, Bioproducts and Biorefining*, 2014, **8**,.

[27] A. Rodríguez, E. Espinosa Víctor, J. Robles, R. Sánchez, I. Bascón Villeas and A. Rosal, in *Different Solvents for Organosolv Pulping*, 2018.

[28] J.-R. Bastidas-Oyanedel and J. Schmidt, 2019.

[29] J. Reiter, H. Strittmatter, L. Wiemann, D. Schieder and V. Sieber, *Green Chem.*, 2013, **15**, 1373–1381.

[30] S. Liu, L. Bai, A. Muyden, Z. Huang, X. Cui, Z. Fei, X. Li, X. Hu and P. Dyson, *Green Chemistry*, 2019, **21**,.

[31] I. Bosque, G. Magallanes, M. Rigoulet, M. Kärkäs and C. Stephenson, *ACS Cent. Sci.*, 2017, **3**,.

[32] A. Berlin and M. Balakshin, *Bioenergy Research: Advances and Applications*, 2014, 315–336.

[33] O. Sánchez, R. Sierra and C. Almeciga-Diaz, in *Delignification Process of Agro-Industrial Wastes an Alternative to Obtain Fermentable Carbohydrates for Producing Fuel*, 2011.

[34] X. Pan, Y. Sano and T. Ito, *Holzforschung*, 1999, **53**, 49–55.

[35] P. Rousu, P. Rousu and J. Anttila, *Resources, Conservation and Recycling*, 2002, **35**, 85–103.

[36] K. S. Patrick, *Journal of Medicinal Chemistry*, 2007, **50**, 1423–1423.

[37] S. Irmak, in *Biomass as Raw Material for Production of High[U+2010]Value Products*, 2017.

[38] L. Hodasova, M. Jablonsky, S. Andrea and A. Haz, *Wood research*, 2015, **60**, 973–986.

[39] I. N. de Estadística y Censos, *Ecuador en cifras*, 2018.

[40] Unknown, in *Mapa de Ecuador en blanco y negro*.

[41] A.-O. A. S. T. D'Orazio J, Jarrett S, *International Journal of Molecular Sciences*, 2013.

[42] M. Parit, P. Saha, V. A. Davis and Z. Jiang, *ACS Omega*, 2018, **3**, year.

[43] W. H. Organization, 2003.

[44] S. C. Foundation, 2019.

[45] M. Neundorf, in *Sunscreen 101: Everything You Need to Know*.

[46] T. Smijs and S. Pavel, *Nanotechnology, science and applications*, 2011, **4**, 95–112.

[47] H. Sadeghifar, R. Venditti, J. Jur, R. Gorga and J. Pawlak, *ACS Sustainable Chemistry Engineering*, 2016, **5**,.

[48] L. Suits and G. Hsuan, *Geotextiles and Geomembranes*, 2003, **21**, 111–122.

[49] A. Koski, K. Yim and S. Shivkumar, *Materials Letters*, 2004, **58**, 493–497.

[50] K. Deshmukh, M. B. Ahamed, R. R. Deshmukh, P. R. Bhagat, S. K. K. Pasha, A. Bhagat, R. Shirbhate, F. Telare and C. Lakhani, *Polymer-Plastics Technology and Engineering*, 2016, **55**, 231–241.

[51] D. N. Watkins, M. V. Hosur, A. Tcherbi-Narteh and S. Jeelani, author, 2015.

[52] A. Sluiter, B. Hames, R. Ruiz, C. Scarlata, J. Sluiter, D. Templeton and D. Crocker, *National Renewable Energy Laboratory*, 2008.

[53] C. Beliciu and C. Moraru, *Journal of dairy science*, 2009, **92**, 1829–39.

[54] T. Jesionowski, *Journal of Materials Processing Technology*, **203**, 121–128.

[55] M. Mozafari, M. Danaei, M. Dehghankhold, S. Ataei, F. Hasanzadeh Davarani, R. Javanmard, A. Dokhani and S. Khorasany, 2018.

[56] J. Hirsch, *Thermo Fisher Scientific., USA*, 2013.

[57] A. V. R. S. T. N. K. K. Kanny, *Microscopy Applied to Materials Sciences and Life Sciences*, Apple Academic Press (TF), 1st edn., 2019.

[58] F. G. S. J. S. T. Aneesa Padinjakkara, Aparna Thankappan, in *Biopolymers and Biomaterials*, 2018.

[59] O. Choudhary and P. Choudhary, *International Journal of Current Microbiology and Applied Sciences*, 2017, **6**, 1877–1882.

[60] F. Sima, C. Ristoscu, D. Liviu, O. Gallet, K. Anselme and I. Mihailescu, in *Laser thin films deposition and characterization for biomedical applications*, 2016, pp. 77–125.

[61] D. Arzensek, *Seminar University of Ljubljana*, 2010, 1–18.

[62] U. Kätzel, R. Bedrich, M. Stintz, R. Ketzmerick, T. Gottschalk-Gaudig and H. Barthel, *Particle   Particle Systems Characterization*, 2008, **25**, 9 – 18.

[63] T. Glawdel and C. Ren, in *Zeta Potential Measurement*, 2015, pp. 3513–3522.

[64] M. Kaszuba, J. Corbett, F. Watson and A. Jones, *Philosophical transactions. Series A, Mathematical, physical, and engineering sciences*, 2010, **368**, 4439–51.

[65] M. Instruments, 2005, 1–.

[66] S.-J. Park and M.-K. Seo, *Interface Science and Composites*, Elsevier, 2011, vol. 18.

[67] M. Shah, M. Imran and S. Ullah, *Lipid-Based Nanocarriers for Drug Delivery and Diagnosis*, 2017, pp. 1–353.

[68] B. Stuart, in *Polymer Analysis*, 2003, pp. 52–54.

[69] O. Ayotunde, W. Cranton and I. Dharmadasa, in *Techniques Utilised in Materials Growth and Materials and Device Characterisation*, 2019, pp. 41–73.

[70] N. S. Murthy, C. Bednarczyk, P. Rim and C. Nelson, *Journal of Applied Polymer Science - J APPL POLYM SCI*, 1997, **64**, 1363–1371.

[71] A. A. Bunaciu, E. UdriSTioiu and H. Aboul-Enein, *Critical reviews in analytical chemistry / CRC*, 2015, **45**,.

[72] L. Mingliu, H. Zhang, H. Zheng, Y. Li, H. Huang and R. Xu, *Chinese Journal of Chemical Engineering*, 2013, **21**, 427–433.

[73] R. Martín-Sampedro, J. Santos, U. Fillat, B. Wicklein, M. Eugenio and D. Ibarra, *International Journal of Biological Macromolecules*, 2019, **126**, 18–29.

[74] L. Zhang, L. Yan, B. Yang and D. Laskar, *Biotechnology for Biofuels*, 2014, **8**,.

[75] A. J. Ragauskas, *Materials for Biofuels*, World Scientific Publishing Company, 1st edn., 2013, vol. 4.

[76] M. Greger, T. Landberg and M. Vaculík, *Plants*, 2018, **7**, 41.

[77] D. Mohan, C. Pittman and P. Steele, *Energy*, 2006, **20**, 848–855.

[78] E. Saliba, N. Rodriguez, D. Piló-Veloso and S. Morais, *Arquivo Brasileiro de Medicina Veterinária e Zootecnia*, 2002, **54**,.

[79] N. Sallem, C. Vanderghem, T. Pacary, A. Richel, D. Debecker, J. Devaux and M. Sclavons, *Polymer Degradation and Stability*, 2016, **130**,.

[80] L. Oliveira, N. Cordeiro, D. Evtuguin, I. Torres and A. Silvestre, *Industrial Crops and Products*, 2007, **26**, 163.

[81] K. Ashraf, M. R. K. Khan, D. Higgins and M. Collinson, *Langmuir*, 2018, **34**,.

[82] M. S. Sujata V. Bhat, B.A. Nagasampagi, *Chemistry of Natural Products*, Springer Science Business Media, 2005, vol. 233-235.

[83] L. Matsakas, A. Karnaouri, A. Cwirzen, U. Rova and P. Christakopoulos, *Molecules*, 2018, **23**, 1822.

[84] M. Lievonen, J. Valle Delgado, M.-L. Mattinen, E.-L. Hult, K. Lintinen, M. Kostiainen, A. Paananen, G. Szilvay, H. Setälä and M. Österberg, *Green Chem.*, 2015, **18**,.

[85] C. Frangville, M. Rutkevicius, A. Richter, O. Velev, S. Stoyanov and V. Paunov, *Chemphyschem : a European journal of chemical physics and physical chemistry*, 2012, **13**,.

[86] T. You and F. Xu, Applications of Molecular Spectroscopy to Current Research in the Chemical and Biological Sciences, 2016.

[87] L. D. S. Yadav, *Organic Spectroscopy*, Springer, 2004, vol. 1.

[88] K. A. Ansari and V. Gaikar, *Chemical Engineering Science*, 2013, **115**, 157–166.

[89] U. Y. . S. Y. Kubo, S., *Journal of Wood Science*, 2003, **49**, 188–19.

[90] G. Rudko, A. Kovalchuk, V. Fediv, J. Beyer, W. Chen and I. Buyanova, *Advanced Science, Engineering and Medicine*, 2012, **4**, 394–400.

[91] Y. Qian, Q. Xueqing and S. Zhu, *Green Chem.*, 2014, **17**,.